Materials and Components
Technology Division
Materials and Components
Technology Division
Materials and Components
Technology Division
Materials and Components
Technology Division
Materials and Components
Technology Division
Materials and Components
Technology Division
Materials and Components
Technology Division
Materials and Components
Technology Division
Materials and Components
Technology Division
Materials and Components
Technology Division
Materials and Components
Technology Division
Materials and Components
Technology Division
Materials and Components
Technology Division
Materials and Components
Technology Division
Materials and Components
Technology Division
Materials and Components
Technology Division
Materials and Components
Technology Division

ANL-90/38

A Theory for Fluidelastic Instability of Tube-Support-Plate Inactive Modes

by Y. Cai, S. S. Chen,
and S. Chandra

Argonne National Laboratory, Argonne, Illinois 60439
operated by The University of Chicago
for the United States Department of Energy under Contract W-31-109-Eng-38

Materials and Components
Technology Division
Materials and Components
Technology Division
Materials and Components
Technology Division
Materials and Components
Technology Division

Argonne National Laboratory, with facilities in the states of Illinois and Idaho, is owned by the United States government, and operated by The University of Chicago under the provisions of a contract with the Department of Energy.

ARGONNE NATIONAL LABORATORY
9700 South Cass Avenue, Argonne, Illinois 60439

ANL–90/38

Distribution
Category:
Industrial Programs
(General) (UC–310)

A Theory for Fluidelastic Instability of Tube–Support–Plate Inactive Modes

---

by

Y. Cai, S. S. Chen, and S. Chandra*

Materials and Components Technology Division

September 1990

Work supported by

NORTHEAST UTILITIES SERVICE COMPANY

U.S. DEPARTMENT OF ENERGY
Office of Conservation and Renewable Energy

---

*Northeast Utilities Service Company, Hartford, Connecticut

Contents

Nomenclature vi

Abstract 1

1 Introduction 1

2 Equations of Motion 3

3 A Bilinear Model for Loosely Supported Tubes 7

4 Modal Analysis 16

5 Simulations of Loosely Held Tubes 22

6 Impact Forces 30

7 Conclusions 33

Acknowledgments 35

References 35

Figures

1 Tube row oscillating in nonuniform crossflow 3

2 Schematic of tube and supports in crossflow 8

3 Schematic of tube with supports C1 and C2, and right end free 8

4 Schematic of tube with supports C1 and C2, and right end supported by a spring 9

5 Relationship of reduced flow velocity and fluid-damping coefficient α'_{11} when pitch-to-diameter ratio is equal to 1.33 15

6 Relationship of reduced flow velocity and fluid-stiffness coefficient α''_{11} when pitch-to-diameter ratio is equal to 1.33 15

7 Mode shapes for Model 1 19

8 Mode shapes for Model 2 20

9 Time histories of tube displacement calculated with various numbers of modes 21

10 Time histories and phase portraits of tube vibration calculated with various numbers of modes 22

11 Mode shapes of tube motion in one cycle 24

12 Modal damping vs. flow velocity 25

13 Oscillation frequency vs. flow velocity 26

14 Displacement and velocity of tube motion at points $z/\ell = 1.0$ and $z/\ell = 0.35$ 27

15 Time histories of displacement and portraits of tube motion at various flow velocities 28

16 RMS tube displacement as a function of flow velocity for various diametral gaps 29

17 RMS tube displacement as a function of flow velocity with a diametral gap of 1.02 mm 29

18 Time histories of tube displacements for various gaps 31

19 PSD of tube displacement for various flow velocities when the diametral gap is 2.54 mm 32

20 Time histories of impact force with various flow velocities 33

21 Time histories of impact force with various asymmetrical gaps at flow velocity U_m = 2.0 m/s 34

Tables

1 Calculated natural frequencies of a tube 18

2 Calculated and measured natural frequencies of a tube 18

3 Impact force and work rate with various flow velocities 32

Nomenclature

A_{jn}	Coefficients
a_{jn}, $\dot{a}_{jn}$	Generalized tube displacement and velocity in x direction
B_{jn}	Coefficients
b_{jn}, $\dot{b}_{jn}$	Generalized tube displacement and velocity in y direction
C_1, C_2	Coefficients
D	Tube diameter
E	Young's modulus
e	Wall thickness of tube
e_1, e_2	Tube-support gaps
F_i	Impact force
f	Oscillation frequency
f_n	Natural frequency of n-th mode
I	Moment of inertia of tube cross section
K_c	Equivalent stiffness
k_{n_1}, k_{n_2}	Eigenvalues for tube vibration
ℓ	Tube length
m_j	Mass per unit length of j-th tube
N	Number of tubes in array or row
n	Number of modes
P	Pitch
R	Radius of tube

T_c	Contact time of tube/support
t	Time
t_s	Time when tube strikes TSP
t_d	Time when tube leaves TSP
U	Flow velocity
U_m	Mean flow velocity
U_r	Reduced flow velocity (= U_m/fD or U/fD)
u_j, $\dot{u}_j$	Displacement and velocity of j-th tube in x direction
u_1, $\dot{u}_1$	Displacement and velocity of tube for TSP-inactive mode
u_2, $\dot{u}_2$	Displacement and velocity of tube for TSP-active mode
v_j, $\dot{v}_j$	Displacement and velocity of j-th tube in y direction
x, y, z	Cartesian coordinates
W_r	Wear work rate parameters
α_{jk}, β_{jk}, σ_{jk}, τ_{jk}	Added-mass coefficients
α'_{jk},β'_{jk}, σ'_{jk},τ'_{jk}	Fluid damping coefficients
α''_{jk},β''_{jk}, σ''_{jk},τ''_{jk}	Fluid stiffness coefficients
ξ, ξ_1, ξ_2	Dimensionless coordinates
ζ_j, η_j	Damping ratio in vacuum
γ_j	Mass ratio (= $\rho\pi R^2/m_j$) of j-th tube

μ, ν	Dimensionless distances
ω	Circular frequency
ω_j, Ω_j	Natural frequency in radian of j-th tube in vacuum
$\varphi_n(z)$	Orthonormal function of n-th mode
$\psi(z)$	Flow velocity distribution function

Subscripts

j,k	Tube number j,k (j,k = 1 to N)
n	n-th modes
1	For Model 1 (TSP-inactive mode)
2	For Model 2 (TSP-active mode)

A Theory for Fluidelastic Instability of Tube–Support–Plate Inactive Modes

by

Y. Cai, S. S. Chen, and S. Chandra

Abstract

Fluidelastic instability of loosely supported tubes, vibrating in a tube-support-plate (TSP) inactive mode, is suspected to be one of the main causes of tube failure in some operating steam generators and heat exchangers. This report presents a mathematical model for fluidelastic instability of loosely supported tubes exposed to nonuniform crossflow. The model incorporates all motion-dependent fluid forces based on the unsteady flow theory. In the unstable region associated with a TSP-inactive mode, tube motion can be described by two linear models: TSP-inactive mode when tubes do not strike the TSP, and TSP-active mode when tubes do strike the TSP. A bilinear model (consisting of these linear models) presented in this report simulates the characteristics of fluidelastic instability of loosely supported tubes in stable and unstable regions associated with TSP-inactive modes. Analytical results obtained with the model are compared with published experimental data; they agree reasonably well. The prediction procedure presented for fluidelastic instability response of loosely supported tubes is applicable to the stable and unstable regions of the TSP-inactive mode.

1 Introduction

Fluidelastic instability associated with a tube-support-plate (TSP) inactive mode for loosely held tubes has been demonstrated in laboratory tests and observed in a few heat exchangers.[1-6] It is suspected to be a main cause of tube failure in some operating steam generators and heat exchangers. The phenomenon occurs as a result of design-inherent clearances between the tubes and their supports, such as baffle plates and antivibration bars. When these tubes are subjected to a cross flow, flow-induced vibration can cause them to strike and rub against their supports, resulting in tube wear. If tube vibration is excessive in duration and amplitude, wear can result in sufficient loss of tube-wall material to cause fatigue cracking and/or tube leaks.

In recent years, extensive experimental and analytical studies have been performed on fluidelastic instability of loosely held tubes and how this instability is related to wear. Chen et al.[1] investigated the fluidelastic behavior of loosely held

tubes in the laboratory. They observed that, as the flow velocity is increased to a threshold value, instability in a TSP-inactive mode may occur. Then, for a range of flow velocities higher than the threshold flow velocity, the tube vibrates predominantly in a TSP-inactive mode, with the response amplitude limited by the clearance between the tube and the TSP. With a further increase of flow velocity, a second threshold, or critical, flow velocity is reached at which instability in a TSP-active mode begins. In this case, large-amplitude oscillations occur and, in many cases, tubes may strike one another.

Additional studies to determine the response of loosely supported tubes under some specific flow conditions have recently been published.[7-16] References 7-11 describe experiments on tubes vibrating in a TSP-inactive mode, dynamic contact forces between tubes and supports, and wear mechanisms. Using both analytical and numerical methods, other investigators[12-21] consider computer simulations of fluidelastic instability of loosely held tubes. For example, Fisher et al.[13] and Rao et al.[12,15] developed finite-element computer codes to simulate tube vibration and fretting wear and compared the results they obtained with the codes with experimental measurements. Nonlinear analytical methods for analyzing the fluidelastic instability and impacting behavior of loosely held tubes are presented by Fricker[14] and Axisa et al.[20] They used quasistatic or quasisteady flow theories, which are applicable in specific parameter ranges. Only the unsteady flow theory is applicable in all cases.[22] A study based on the unsteady flow model has also been conducted on fluidelastic instability of tubes in nonuniform flow.[23]

The objective of this work is to develop an analytical model for predicting tube response of loosely held tube arrays in crossflow. This report describes an analytical/numerical procedure for predicting the critical flow velocity and tube response in the instability region associated with a TSP-inactive mode. First, fluid coupling effects among tubes, including fluid inertia, fluid damping, and fluid stiffness, are described by the unsteady flow theory. At present, very limited data are available for these fluid-force coefficients. In this work, we used the coefficients presented in Ref. 23, which are based on the experimental data of Tanaka.[24] Second, as in the first step, all TSPs are considered as elastic stops, and fluid effects are not included. In the future, an analytical or empirical model, based on published experimental data[7-11] can be incorporated into this theory. Finally, the coupled tube/flow system is reduced to a bilinear model, which can be solved analytically.

Many calculations have been carried out to predict tube displacements, including time histories and frequency spectra. Root-mean-square (RMS) tube displacements as a function of flow velocity for various clearances agree reasonably well with the experimental data of Chen et al.[1] Impact forces at supports due to tube/support interaction associated with the instability of a TSP-

inactive mode are also calculated to correlate them with the wear work-rate parameter. Comparisons of the analytical/numerical results with experimental data show that the unsteady flow theory and bilinear model presented in this report are adequate to describe the nonlinear behavior of fluidelastic instability associated with TSP-inactive modes of loosely supported tube arrays in crossflow. The model can be applied to tube vibration and wear in steam generators and shell-and-tube heat exchangers.

2 Equations of Motion

An unsteady flow theory for fluidelastic instability of tubes in crossflow has been described in detail by Chen[22] and Chen and Chandra.[23] For the sake of completeness, the unsteady flow model for fluidelastic instability of loosely supported tubes is briefly described here.

Consider a row of N tubes oscillating in a flow, Fig. 1. The axes of the tubes are parallel to the z axis. The subscript j is used to denote variables associated with a tube j. Tube displacement components in the x and y directions are u_j and v_j, respectively. The orthonormal modal function of the tube vibrating in vacuum and in fluid is $\varphi_n(z)$:

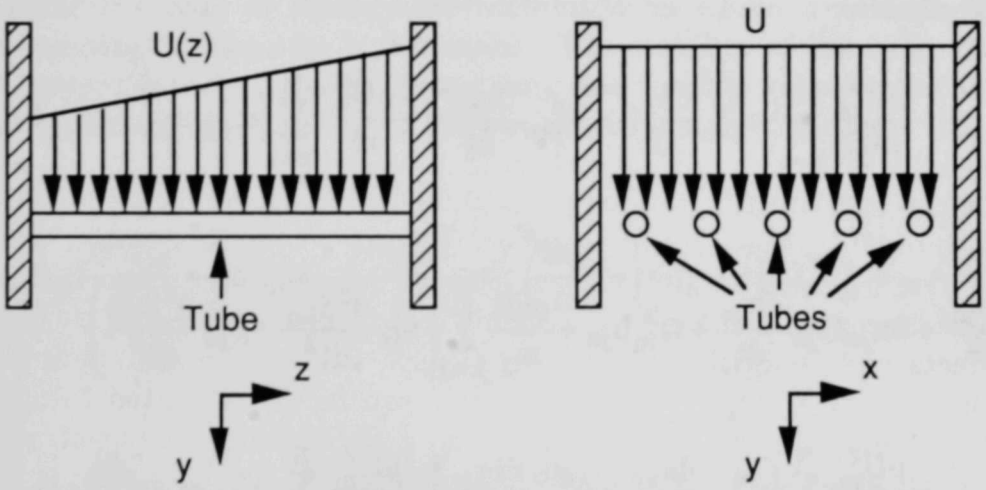

Fig. 1. Tube row oscillating in nonuniform crossflow; U(z) is flow velocity distribution

$$\frac{1}{\ell}\int_0^{\ell}\varphi_n^2(z)dz = 1, \tag{1}$$

where ℓ is the length of the tubes. Let

$$u_j(z,t) = \sum_{n=1}^{\infty} a_{jn}(t)\varphi_n(z),$$

and (2)

$$v_j(z,t) = \sum_{n=1}^{\infty} b_{jn}(t)\varphi_n(z),$$

where $a_{jn}(t)$ and $b_{jn}(t)$ are functions of time only. Assume that the flow velocity distribution is given by

$$U(z) = U_m\psi(z), \tag{3}$$

where U_m is mean flow velocity and $\psi(z)$ is the flow velocity distribution function.

The equations of motion for the tubes are

$$\frac{d^2a_{jn}}{dt^2} + 2\zeta_{jn}\omega_{jn}\frac{da_{jn}}{dt} + \omega_{jn}^2 a_{jn} + \frac{\rho\pi R^2}{m_j}\sum_{k=1}^{N}\left(\alpha_{jk}\frac{d^2a_{kn}}{dt^2} + \sigma_{jk}\frac{d^2b_{kn}}{dt^2}\right)$$

$$-\frac{\rho U_m^2}{m_j\omega}\sum_{k=1}^{N}\left(\alpha_{jkn}^{d}\frac{da_{kn}}{dt} + \sigma_{jkn}^{d}\frac{db_{kn}}{dt}\right) - \frac{\rho U_m^2}{m_j}\sum_{k=1}^{N}\left(\alpha_{jkn}^{e}a_{kn} + \sigma_{jkn}^{e}b_{kn}\right) = 0,$$

and (4)

$$\frac{d^2b_{jn}}{dt^2} + 2\eta_{jn}\Omega_{jn}\frac{db_{jn}}{dt} + \Omega_{jn}^2 b_{jn} + \frac{\rho\pi R}{m_j}\sum_{k=1}^{N}\left(\tau_{jk}\frac{d^2a_{kn}}{dt^2} + \beta_{jk}\frac{d^2b_{kn}}{dt^2}\right)$$

$$-\frac{\rho U_m^2}{m_j\omega}\sum_{k=1}^{N}\left(\tau_{jkn}^{d}\frac{da_{kn}}{dt} + \beta_{jkn}^{d}\frac{db_{kn}}{dt}\right) - \frac{\rho U_m^2}{m_j}\sum_{k=1}^{N}\left(\tau_{jkn}^{e}a_{kn} + \beta_{jkn}^{e}b_{kn}\right) = 0,$$

where ρ is fluid density; R is tube radius; ω is the radian frequency; ζ_{jn} and η_{jn} are damping ratios in vacuum; ω_{jn} and Ω_{jn} are natural frequencies in the radian of the j-th cylinder in vacuum; m_j is cylinder mass per unit length of cylinder j, and

$$\alpha^{d}_{jkn} = \frac{1}{\ell}\int_0^{\ell} \alpha'_{jk}\varphi_n^2(z)\psi^2(z)dz, \qquad \alpha^{e}_{jkn} = \frac{1}{\ell}\int_0^{\ell} \alpha''_{jk}\varphi_n^2(z)\psi^2(z)dz,$$

$$\sigma^{d}_{jkn} = \frac{1}{\ell}\int_0^{\ell} \sigma'_{jk}\varphi_n^2(z)\psi^2(z)dz, \qquad \sigma^{e}_{jkn} = \frac{1}{\ell}\int_0^{\ell} \sigma''_{jk}\varphi_n^2(z)\psi^2(z)dz,$$

$$\tau^{d}_{jkn} = \frac{1}{\ell}\int_0^{\ell} \tau'_{jk}\varphi_n^2(z)\psi^2(z)dz, \qquad \tau^{e}_{jkn} = \frac{1}{\ell}\int_0^{\ell} \tau''_{jk}\varphi_n^2(z)\psi^2(z)dz, \tag{5}$$

$$\beta^{d}_{jkn} = \frac{1}{\ell}\int_0^{\ell} \beta'_{jk}\varphi_n^2(z)\psi^2(z)dz, \qquad \beta^{e}_{jkn} = \frac{1}{\ell}\int_0^{\ell} \beta''_{jk}\varphi_n^2(z)\psi^2(z)dz.$$

Note that α_{jk}, σ_{jk}, τ_{jk}, and β_{jk} are added-mass coefficients; α'_{jk},σ'_{jk},τ'_{jk}, and β'_{jk} are fluid-damping coefficients; and α''_{jk},σ''_{jk},τ''_{jk}, and β''_{jk} are fluid-stiffness coefficients. All these force coefficients are based on the experimental data of Tanaka[24] and have been compiled and evaluated by Chen and Chandra[23] and Chen and Jendrzejczyk.[25]

Equations 4 and 5 are applicable to tube arrays in which all tubes have the same length and same type of boundary conditions. For a group of N tubes, corresponding to each n-th mode for a single tube, there are 2N coupled modes. Based on Eqs. 4, different types of instability can be analyzed, including coupled- and single-mode flutter, or velocity- and displacement-controlled mechanisms.

Consider the case of fluidelastic instability in which a velocity-controlled, negative damping mechanism is dominant. The stability of the tube row may be analyzed approximately by considering only one flexible tube among other rigid tubes and neglecting the coupling in the two directions. For this case, Eqs. 4 can be written as

$$\left(1+\gamma_j\alpha_{jj}\right)\frac{d^2a_{jn}}{dt^2} + \left(2\zeta_{jn}\omega_{jn} - \frac{\gamma_j U_r^2}{\pi^3}\omega\alpha^{d}_{jj}\right)\frac{da_{jn}}{dt} + \left(\omega_{jn}^2 - \frac{\gamma_j}{\pi^3}U_r^2\alpha^{e}_{jj}\right)a_{jn} = 0,$$

and (6)

$$\left(1+\gamma_j\beta_{jj}\right)\frac{d^2b_{jn}}{dt^2} + \left(2\eta_{jn}\Omega_{jn} - \frac{\gamma_j U_r^2}{\pi^3}\omega\beta^{d}_{jj}\right)\frac{db_{jn}}{dt} + \left(\Omega_{jn}^2 - \frac{\gamma_j}{\pi^3}U_r^2\beta^{e}_{jj}\right)b_{jn} = 0,$$

$j = 1, 2, 3, \ldots N, \quad n = 1, 2, 3, \ldots \infty,$

where

$$\gamma_j = \frac{\rho \pi R^2}{m_j} \tag{7}$$

and

$$U_r = \frac{\pi U_m}{\omega R}. \tag{8}$$

Then, the solution of Eqs. 6 can easily be analyzed. For example, the solution of $a_{jn}(t)$ is

$$a_{jn}(t) = e^{-A_{jn}t}\left[C_1 \cos\left(B_{jn}t\right) + C_2 \sin\left(B_{jn}t\right)\right] \tag{9}$$

and

$$\dot{a}_{jn}(t) = -A_{jn}a_{jn}(t) - B_{jn}e^{-A_n t}\left[C_1 \sin\left(B_{jn}t\right) - C_2 \cos\left(B_{jn}t\right)\right],$$

where C_1 and C_2 are coefficients that depend on initial conditions, and

$$A_{jn} = \frac{2\zeta_{jn}\omega_{jn} - \dfrac{\gamma_j U_r^2}{\pi^3}\omega\alpha_{jj}^d}{2\left(1+\gamma_j\alpha_{jj}\right)}, \tag{10}$$

$$B_{jn} = \frac{\left[-\left(2\zeta_{jn}\omega_{jn} - \dfrac{\gamma_j U_r^2}{\pi^3}\omega\alpha_{jj}^d\right)^2 + 4\left(1+\gamma_j\alpha_{jj}\right)\left(\omega_{jn}^2 - \dfrac{\gamma_j}{\pi^3}U_r^2\alpha_{jj}^e\right)\right]^{1/2}}{2\left(1+\gamma_j\alpha_{jj}\right)},$$

and

$$\omega = \sqrt{\frac{\omega_{jn}^2 - \dfrac{\gamma_j}{\pi^3}U_r^2\alpha_{jj}^e}{1+\gamma_j\alpha_{jj}}}. \tag{11}$$

Notice that ω depends on the coefficients α_{jj}^e, which depend on the reduced flow velocity U_r (= U_m/fD = $U_m \cdot 2\pi/\omega D$). Therefore, an iterated method is required to calculate ω.

The displacement and velocity of the tube will be

$$u_j(z,t) = \sum_{n=1}^{\infty} a_{jn}(t)\varphi_n(z)$$

and (12)

$$\dot{u}_j(z,t) = \sum_{n=1}^{\infty} \dot{a}_{jn}(t)\varphi_n(z).$$

3 A Bilinear Model for Loosely Supported Tubes

A two-span flexible tube with one intermediate support in a row of rigid tubes, schematically shown in Fig. 2, was tested by Chen et al.[1] When the right end (C3) of the tube does not strike the stop, it is a pinned-pinned-free model (Model 1, Fig. 3). When the right end strikes the stop, it becomes a pinned-pinned-spring-supported model (Model 2, Fig. 4), where a spring at C3 is used to represent tube/support interaction when the tube strikes the stop.

Vibration of the tube can be represented by a bilinear model consisting of Models 1 and 2. In Model 1, as the displacement of the tube increases, its right end may strike the stop. Once the right end strikes the stop, Model 1 becomes Model 2. Due to increased system stiffness, the tube motion is stabilized and its right end leaves the stop and returns to Model 1.

These two models of tube vibration can be analyzed in two different time regions.

For Model 1, if we assume that during the time interval $0 \le t \le t_s$, the tube displacements at C3 are within the stop limits $-e_2 < u(\ell,t) < e_1$, the boundary conditions at C1 and C3 (Fig. 3) are

$$u(\xi_1,t)\big|_{\xi_1=0} = 0,$$

$$\frac{\partial^2 u}{\partial \xi_1^2}(\xi_1,t)\Big|_{\xi_1=0} = 0,$$

(13)

$$\frac{\partial^2 u}{\partial \xi_2^2}(\xi_2,t)\Big|_{\xi_2=0} = 0,$$

$$\frac{\partial^3 u}{\partial \xi_2^3}(\xi_2,t)\Big|_{\xi_2=0} = 0,$$

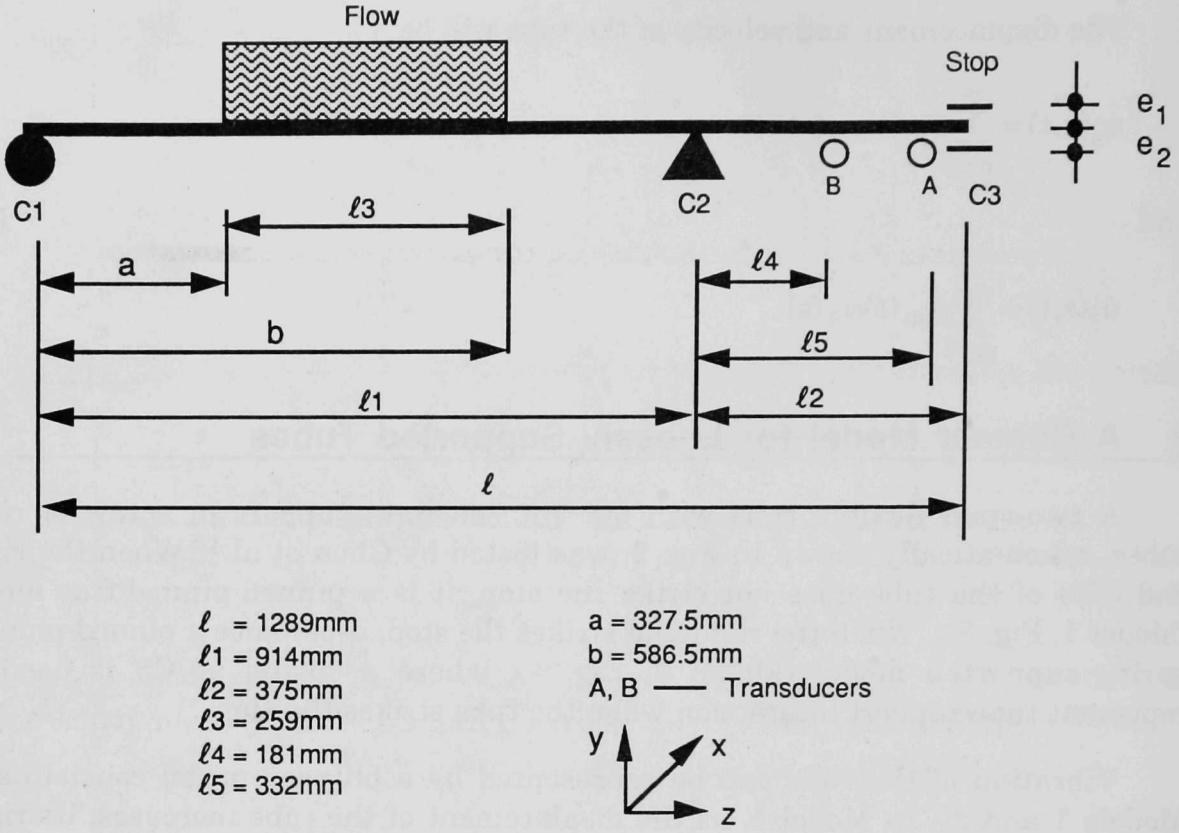

Fig. 2. Schematic of tube and supports (C1 and C2) in crossflow; e_1 and e_2 are stop limits

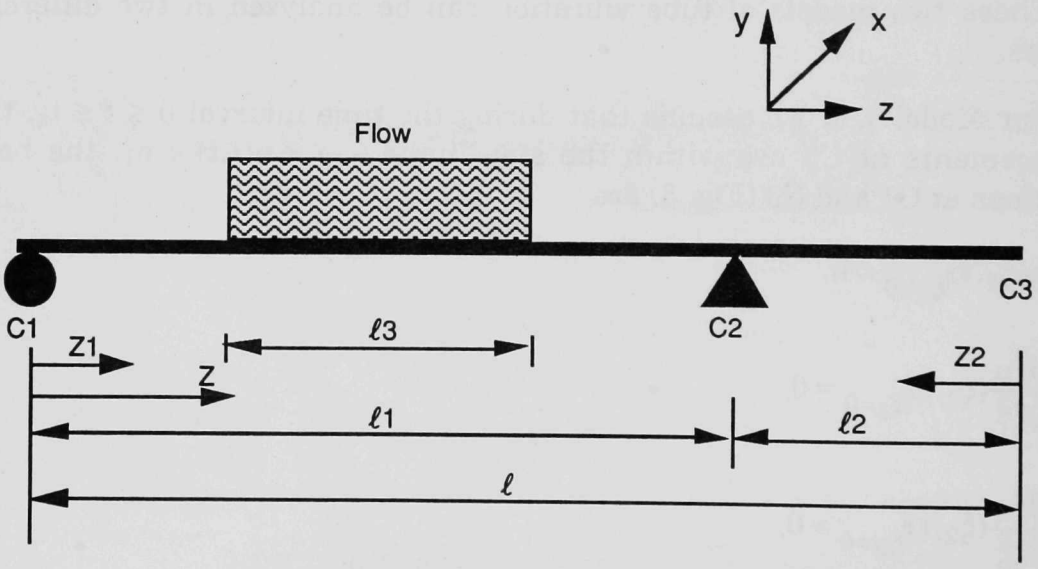

Fig. 3. Schematic of tube with supports C1 and C2, and right end free

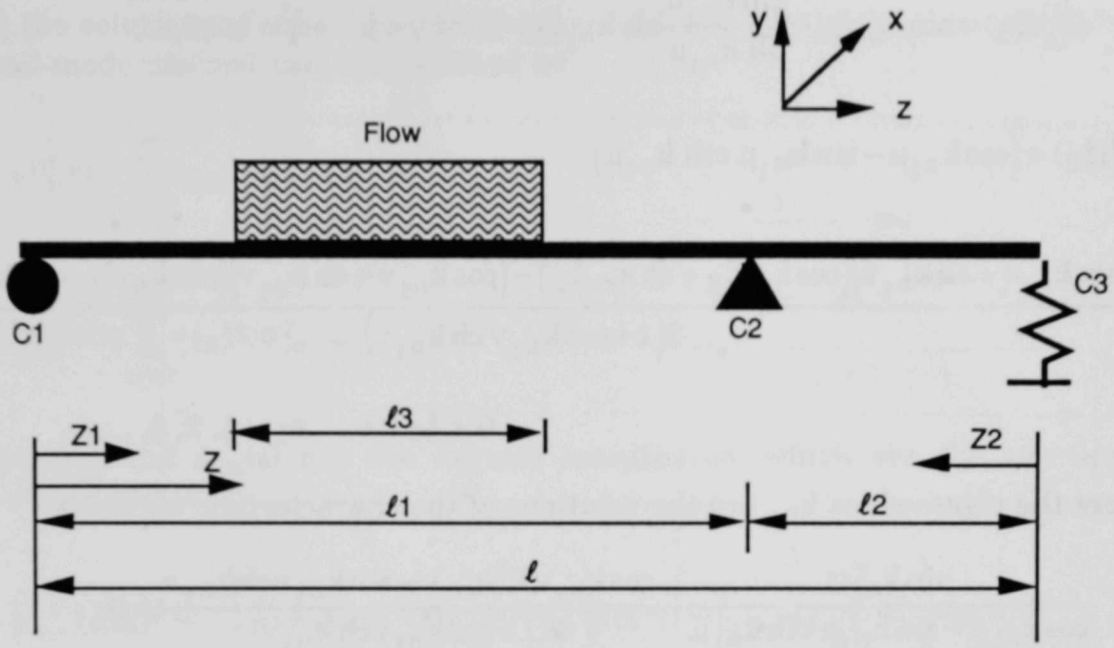

Fig. 4. Schematic of tube with supports C1 and C2, and right end supported by a spring

and the continuous conditions at the intermediate point C2 are

$$u(\xi_1,t)\big|_{\xi_1=\mu} = u(\xi_2,t)\big|_{\xi_2=\nu} = 0,$$

$$\frac{d\varphi_{1n}^{(1)}(\mu)}{d\xi_1} = -\frac{d\varphi_{1n}^{(2)}(\nu)}{d\xi_2}, \tag{14}$$

$$\frac{d^2\varphi_{1n}^{(1)}(\mu)}{d\xi_1^2} = -\frac{d^2\varphi_{1n}^{(2)}(\nu)}{d\xi_2^2},$$

where ξ_1, ξ_2, μ, and ν are dimensionless distances

$$\xi_1 = z_1/\ell\,, \qquad \xi_2 = z_2/\ell\,, \tag{15}$$

$$\mu = \ell_1/\ell\,, \qquad \nu = \ell_2/\ell\,.$$

The functions $\varphi_{1n}^{(1)}$ and $\varphi_{1n}^{(2)}$ are normal modes of Model 1

$$\varphi_{1n}^{(1)}(\xi_1) = \sin k_{n_1}\xi_1 - \frac{\sin k_{n_1}\mu}{\operatorname{sh} k_{n_1}\mu}\operatorname{sh} k_{n_1}\xi_1, \quad 0 < \xi_1 < \mu, \quad n_1 = 1,2,3,..., \tag{16}$$

$$\varphi_{1n}^{(2)}(\xi_2) = \left(\cos k_{n_1}\mu - \sin k_{n_1}\mu \operatorname{cth} k_{n_1}\mu\right)\cdot$$

$$\frac{\left[\left(\sin k_{n_1}\nu + \operatorname{sh} k_{n_1}\nu\right)\left(\cos k_{n_1}\xi_2 + \operatorname{ch} k_{n_1}\xi_2\right) - \left(\cos k_{n_1}\nu + \operatorname{ch} k_{n_1}\nu\right)\left(\sin k_{n_1}\xi_2 + \operatorname{sh} k_{n_1}\xi_2\right)\right]}{2\left(1 + \cos k_{n_1}\nu \operatorname{ch} k_{n_1}\nu\right)}, \tag{17}$$

$$0 < \xi_2 < \nu, \quad n_1 = 1, 2, 3, ...,$$

where the eigenvalues k_{n_1} are the solutions of the characteristic equation

$$\frac{\sin k_{n_1}\mu}{\cos k_{n_1}\mu - \sin k_{n_1}\mu \operatorname{cth} k_{n_1}\mu} - \frac{\cos k_{n_1}\nu \operatorname{sh} k_{n_1}\nu - \sin k_{n_1}\nu \operatorname{ch} k_{n_1}\nu}{2(1 + \cos k_{n_1}\nu \operatorname{ch} k_{n_1}\nu)} = 0. \tag{18}$$

Let

$$\varphi_{1n}(\xi) = \begin{cases} C_{1n}\varphi_{1n}^{(1)}(\xi) & 0 < \xi < \mu \\ C_{1n}\varphi_{1n}^{(2)}(1-\xi) & \mu < \xi < 1, \end{cases}$$

$$\xi = z/\ell\,, \tag{19}$$

where

$$C_{1n} = \frac{1}{\sqrt{\int_0^{\mu}\left[\varphi_{1n}^{(1)}(\xi_1)\right]^2 d\xi_1 + \int_0^{\nu}\left[\varphi_{1n}^{(2)}(\xi_2)\right]^2 d\xi_2}}. \tag{20}$$

Assume that the initial conditions of Model 1 are

$$u(\xi,t)\big|_{t=0} = u_1(\xi),$$

$$\frac{\partial u}{\partial t}(\xi,t)\bigg|_{t=0} = \dot{u}(\xi,t)\bigg|_{t=0} = \dot{u}_1(\xi). \tag{21}$$

Then the solutions of tube vibration (here considered only in the x direction) by the normal-mode method can be described as

$$\left.\begin{aligned} u(\xi,t) &= \sum_{n=1}^{\infty} a_{1n}(t)\varphi_{1n}(\xi) \\ \dot{u}(\xi,t) &= \sum_{n=1}^{\infty} \dot{a}_{1n}(t)\varphi_{1n}(\xi) \end{aligned}\right\} \quad 0 < t < t_s, \tag{22}$$

where a_{1n} and $\dot{a}_{1n}(t)$ are the normal coordinates, which are the solutions of following equations:

$$\left(1+\gamma_j\alpha_{jj}\right)\ddot{a}_{1n} + \left(2\xi_{jn_1}\omega_{jn_1} - \gamma_j\frac{U_r^2}{\pi^3}\omega\alpha_{jj}^d\right)\dot{a}_{1n} + \left(\omega_{jn_1}^2 - \gamma_j\frac{U_r^2}{\pi^3}\alpha_{jj}^e\right)a_{1n} = 0, \tag{23}$$

$$a_{1n}(0) = \int_0^1 u_1(\xi)\varphi_{1n}(\xi)d\xi, \tag{24}$$

$$\dot{a}_{1n}(0) = \int_0^1 \dot{u}_1(\xi)\varphi_{1n}(\xi)d\xi. \tag{25}$$

When $t = t_s$, the right end of the tube strikes the stop and it becomes Model 2, i.e.,

$$u(\xi,t)\big|_{\xi=1} = e_1, \quad \text{or} \quad u(\xi,t)\big|_{\xi=1} = -e_2, \quad t_s < t < t_d, \tag{26}$$

where t_d is the time when the tube leaves the stop at C3.

The displacement and velocity of the tube at t_s are taken as the initial conditions of Model 2, hence,

$$\left.\begin{aligned} u(\xi,t)\big|_{t=t_s} &= \sum_{n=1}^{\infty} a_{1n}(t_s)\varphi_{1n}(\xi) = u_2(\xi), \\ \dot{u}(\xi,t)\big|_{t=t_s} &= \sum_{n=1}^{\infty} \dot{a}_{1n}(t_s)\varphi_{1n}(\xi) = \dot{u}_2(\xi). \end{aligned}\right. \tag{27}$$

The boundary conditions of Model 2 for $t_s < t < t_d$ are

$$u(\xi_1,t)\big|_{\xi_1=0}=0,$$

$$\frac{\partial^2 u}{\partial \xi_1^2}(\xi_1,t)\bigg|_{\xi_1=0}=0,$$

$$\frac{\partial^2 u}{\partial \xi_2}(\xi_2,t)\bigg|_{\xi_2=0}=0, \tag{28}$$

$$\frac{\partial^3 u}{\partial \xi_2^3}(\xi_2,t)\bigg|_{\xi_2=0}=\frac{K_c}{EI}u(\xi_2,t)\bigg|_{\xi_2=0},$$

where K_c is the equivalent stiffness, E is Young's modulus, and I is the moment of inertia.

The continuous conditions at the intermediate point C2 are

$$u(\xi_1,t)\big|_{\xi_1=\mu}=u(\xi_2,t)\big|_{\xi_2=\nu}=0,$$

$$\frac{d\varphi_{2n}^{(1)}(\mu)}{d\xi_1}=-\frac{d\varphi_{2n}^{(2)}(\nu)}{d\xi_2}, \tag{29}$$

$$\frac{d^2\varphi_{2n}^{(1)}(\mu)}{d\xi_1}=\frac{d^2\varphi_{2n}^{(2)}(\nu)}{d\xi_2}.$$

The functions $\varphi_{2n}^{(1)}$ and $\varphi_{2n}^{(2)}$ are normal modes of Model 2

$$\varphi_{2n}^{(1)}(\xi_1)=\sin k_{n_2}\xi_1-\frac{\sin k_{n_2}\mu}{\operatorname{sh} k_{n_2}\mu}\operatorname{sh} k_{n_2}\xi_1,\quad 0<\xi_1<\mu,\quad n_2=1,2,3,\ldots, \tag{30}$$

and

$$\varphi_{2n}^{(2)}(\xi_2)=D_{1n}\Big[D_{2n}\left(\sin k_{n_2}\xi_2+\operatorname{sh} k_{n_2}\xi_2\right)+D_{3n}\left(\cos k_{n_2}\xi_2+\operatorname{ch} k_{n_2}\xi_2\right)$$

$$+D_{4n}\sin k_{n_2}\xi_2+D_{5n}\operatorname{sh} k_{n_2}\xi_2\Big],\quad 0<\xi_2<\nu,\quad n_2=1,2,3,\ldots, \tag{31}$$

where

$$D_{1n} = \frac{\cos k_{n_2}\mu - \sin k_{n_2}\mu \operatorname{cth} k_{n_2}\mu}{2\left(1+\cos k_{n_2}\nu \operatorname{ch} k_{n_2}\nu\right)+\dfrac{2K_c}{EI}\dfrac{1}{k_{n_2}^3}\left(\cos k_{n_2}\nu \operatorname{sh} k_{n_2}\nu - \sin k_{n_2}\nu \operatorname{ch} k_{n_2}\nu\right)},$$

$$D_{2n} = \cos k_{n_2}\nu + \operatorname{ch} k_{n_2}\nu,$$

$$D_{3n} = -\left(\sin k_{n_2}\nu + \operatorname{sh} k_{n_2}\nu\right),$$

$$D_{4n} = -\frac{2K_c}{EI}\frac{1}{k_{n_2}^3}\operatorname{sh} k_{n_2}\nu,$$

$$D_{5n} = \frac{2K_c}{EI}\frac{1}{k_{n_2}^3}\sin k_{n_2}\nu,$$

$n_2 = 1, 2, 3, \ldots,$

where k_{n_2} are the solutions of the characteristic equation.

$$\frac{\sin k_{n_2}\mu}{\cos k_{n_2}\mu - \sin k_{n_2}\mu \operatorname{cth} k_{n_2}\mu} + \frac{\sin k_{n_2}\nu}{\cos k_{n_2}\nu - \sin k_{n_2}\nu \operatorname{cth} k_{n_2}\nu} = 0. \tag{32}$$

Let

$$\varphi_{2n}(\xi) = \begin{cases} C_{2n}\varphi_{2n}^{(1)}(\xi) & 0 < \xi < \mu \\ C_{2n}\varphi_{2n}^{(2)}(1-\xi) & \mu < \xi < 1, \end{cases} \tag{33}$$

$$C_{2n} = \frac{1}{\sqrt{\int_0^{\mu}\left[\varphi_{2n}^{(1)}(\xi_1)\right]^2 d\xi_1 + \int_0^{\nu}\left[\varphi_{2n}^{(2)}(\xi_2)\right]^2 d\xi_2}}. \tag{34}$$

The solutions of the tube vibration by the normal-mode method are

$$\left.\begin{aligned} u(\xi,t) &= \sum_{n=1}^{\infty} a_{2n}(t)\varphi_{2n}(\xi) + u_2(\xi) \\ \dot{u}(\xi,t) &= \sum_{n=1}^{\infty} \dot{a}_{2n}(t)\varphi_{2n}(\xi) \end{aligned}\right\} t_s < t < t_d, \tag{35}$$

where $a_{2n}(t)$ and $\dot{a}_{2n}(t)$ are the solutions of following equations:

$$\left(1+\gamma_j\alpha_{jj}\right)\ddot{a}_{2n} + \left(2\zeta_{jn_2}\omega_{jn_2} - \gamma_j\frac{U_r^2}{\pi^3}\omega\alpha_{jj}^{d}\right)\dot{a}_{2n} + \left(\omega_{jn_2}^2 - \gamma_j\frac{U_r^2}{\pi^3}\alpha_{jj}^{e}\right)a_{2n} = 0 \tag{36}$$

$$a_{2n}(0) = 0 \tag{37}$$

$$\dot{a}_{2n}(0) = \int_0^1 \dot{u}_2(\xi)\varphi_{2n}(\xi)d\xi. \tag{38}$$

The flow-velocity distribution in Fig. 2 can be defined as

$$\psi(\xi) = \begin{cases} 0 & 0 < \xi < \xi_a \\ 1 & \xi_a < \xi < \xi_b \\ 0 & \xi_b < \xi < 1 \end{cases} \tag{39}$$

$$\xi_a = a/\ell\,, \qquad \xi_b = b/\ell\,.$$

Therefore, the force coefficients α_{jj}^{d} and α_{jj}^{e} in Eqs. (23) and (36) will be

$$\begin{aligned} \alpha_{jj}^{d} &= \int_0^1 \alpha_{jj}'\varphi^2(\xi)\psi^2(\xi)d\xi = \alpha_{jj}'\int_0^1 \varphi^2(\xi)\psi^2(\xi)d\xi \\ \alpha_{jj}^{e} &= \int_0^1 \alpha_{jj}''\varphi^2(\xi)\psi^2(\xi)d\xi = \alpha_{jj}''\int_0^1 \varphi^2(\xi)\psi^2(\xi)d\xi, \end{aligned} \tag{40}$$

$$\varphi(\xi) = \begin{cases} \varphi_{1n}(\xi) & 0 < t < t_s \\ \varphi_{2n}(\xi) & t_s < t < t_d, \end{cases} \tag{41}$$

where α_{jj}' and α_{jj}'' are fluid-damping and fluid-stiffness coefficients, which are functions of reduced flow velocity U_r. Figures 5 and 6 show the relationships of these coefficients to U_r (j = 1).

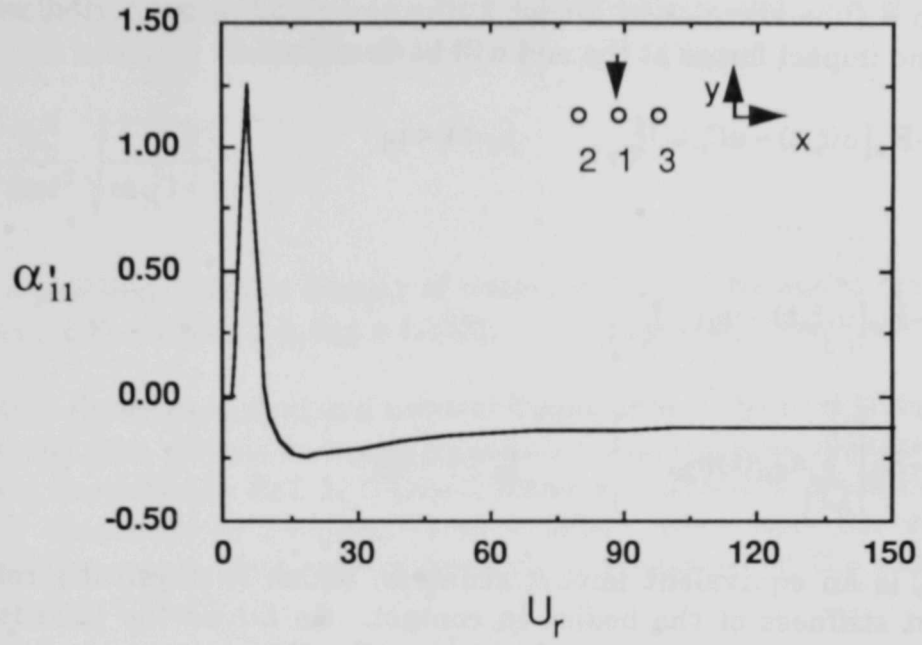

Fig. 5. Relationship of reduced flow velocity and fluid-damping coefficient α'_{11} when pitch-to-diameter ratio is equal to 1.33

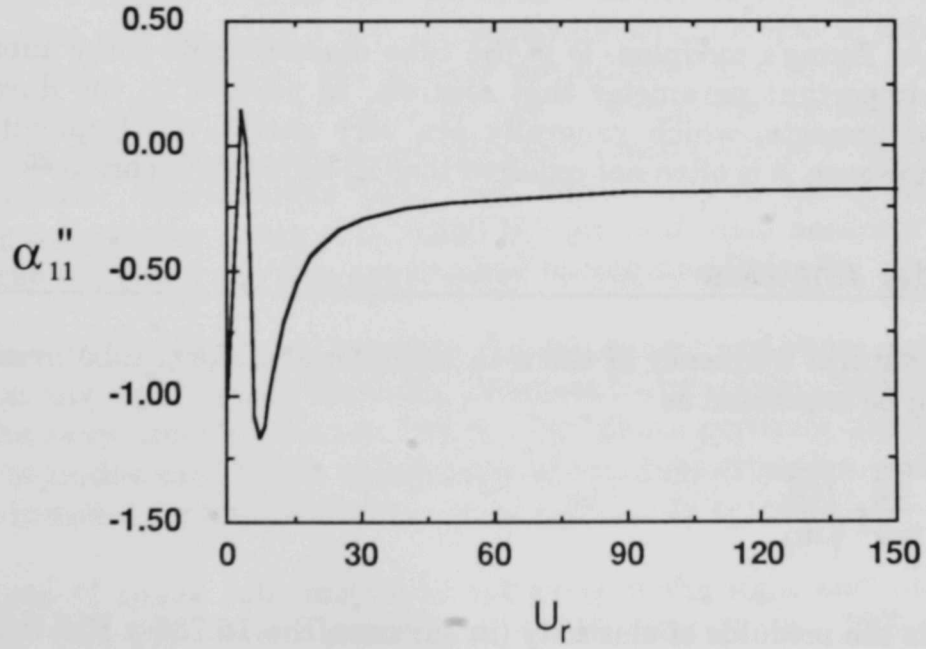

Fig. 6. Relationship of reduced flow velocity and fluid-stiffness coefficient α''_{11} when pitch-to-diameter ratio is equal to 1.33

When a tube vibrates in Model 2, the right end is supported with a spring (Fig. 4), and impact forces at the end will be described as

$$F_i = -K_c[u(\xi,t) - u(\xi,t_s)]\Big|_{\xi=1} \qquad t_s < t < t_d \tag{42}$$

or

$$F_i = -K_c[u(\xi,t) - u_2(\xi)]\Big|_{\xi=1}$$

$$= -K_c\left[\sum_{n=1}^{\infty} a_{2n}(t)\varphi_{2n}(1)\right] \qquad t_s < t < t_d, \tag{43}$$

where K_c is an equivalent impact stiffness, which is physically related to the equivalent stiffness of the bodies in contact. As far as the tube is concerned, satisfactory results can be obtained by using the stiffness associated with the local evaluation [20]

$$K_c = 1.9\frac{Ee^2}{D}\sqrt{\frac{e}{D}}, \tag{44}$$

where E is Young's modulus, D is the tube diameter and e the tube thickness. K_c is an important parameter that controls, in particular, the duration of the individual impacts, which generally are very short-lived (typically less than 10^{-3} s). However, it is often not required that K_c be highly accurate.[20]

4 Modal Analysis

The natural frequency of the n-th mode for a uniform tube in air, shown in Fig. 2, can be expressed as

$$f_n = \frac{k_n^2}{2\pi\ell^2}\sqrt{\frac{EI}{m_j}}, \tag{45}$$

where E is the modulus of elasticity (in our case, E = 15.786 x 10^{-6} lb/in.^{2}), I is the area moment of inertia of the cross section about the neutral axis (tube parameters, R = 0.016 m, e = 0.00159 m), ℓ is tube length, m_j is the mass per unit length, and k_n is a dimensionless parameter that is related to the mode numbers and boundary conditions. In our case, k_n can be calculated from the characteristic equations according to Models 1 and 2 described in Section 3.

If a tube is submerged in water, the added mass of water on the tube should be taken into account. Then, Eq. 45 becomes

$$f_n = \frac{k_n^2}{2\pi\ell^2}\sqrt{\frac{EI}{m_j\left(1+\gamma_j\alpha_{jj}\right)}}, \tag{46}$$

where $\gamma_j = \rho\pi R^2/m_j$, ρ is the density of water, and α_{jj} is the added-mass coefficient (in our case, P/D = 1.33, j = 1, α_{11} = 1.113).

Table 1 shows the calculated natural frequencies of the first 10 modes for both Models 1 and 2 in air and in water, based on the system parameters given in the experiment described in Ref. 1. Table 2 shows a comparison of the calculated and measured fundamental frequencies of a tube. Note that the values of the calculated frequencies are very close to those measured in the experiments for both for Models 1 and 2.

Figures 7 and 8 show the normal mode shapes of the first 10 modes for Models 1 and 2, respectively. These mode shapes depend on the parameters of the tube span given in Figs. 3 and 4.

Figure 9 shows the time histories of tube motion at the right end (C3) when $e_1 = e_2$ = 1.54 mm, calculated with different numbers of modes at the flow velocity U_m = 2.0 m/s. Obviously, the greater the number of modes taken, the more accurate the simulation of tube motion. When the number of modes is insufficient, the contact time in the TSP-active mode will be long (see flat top of displacement). Calculations have been carried out to verify that 10 modes (covering a frequency range of 0-15,000 Hz) give sufficient accuracy for our case. Time-steps of 5×10^{-5} s or less are required during simulation for 10 modes.

Figure 10 gives the time histories of displacement and phase portraits of tube motion at the right end of the tube, calculated with various numbers of modes under the same conditions as in Fig. 9. The phase portraits illustrate that the number of modes used in the calculations affects tube vibration, and more modes must be included for the simulations to be sufficiently accurate.

Figure 11 shows tube motion in one cycle at the right end, at flow velocity U_m = 2.0 m/s; the motion includes both TSP-inactive and TSP-active modes. Figure 11a is calculated with one mode; Fig. 11b is calculated with five modes. When the right end of the tube strikes the stop, the tube will continue its motion except for the right end, which is restrained by a high-stiffness spring support. Figure 11b shows a complicated mode shape that was obtained with more modes.

Table 1. Calculated natural frequencies of a tube

Models	n	k	In Air		In Water	
			ω (rad)	f (Hz)	ω (rad)	f (Hz)
Model 1 TSP-inactive	1	3.90	166	26.5	143	22.7
	2	5.87	377	60	323	51.4
	3	9.46	979	156	839	133
	4	13.4	1950	310	1670	266
	5	15.2	2528	402	2164	345
	6	18.4	3708	590	3176	505
	7	22.5	5548	883	4752	756
	8	25.4	7075	1126	6059	964
	9	27.5	8291	1320	7102	1130
	10	31.5	10876	1731	9315	1483
Model 2 TSP-active	1	5.08	282	44.9	242	38.5
	2	9.20	926	147	793	126
	3	12	1562	249	1338	213
	4	14.2	2200	350	1884	300
	5	18.2	3628	577	3107	495
	6	21.8	5194	827	4449	708
	7	23.4	6011	957	5148	819
	8	27.2	8070	1284	6912	1100
	9	31.0	10520	1674	9010	1434
	10	32.7	11669	1857	9995	1591

Table 2. Calculated and measured natural frequencies of a tube (Hz)

Models	In Air		In Water	
	Calculated	Measured	Calculated	Measured
Model 1 (TSP-inactive)	26.48	26.50	22.68	22.70
Model 2 (TSP-active)	44.93	45.40	38.49	38.54

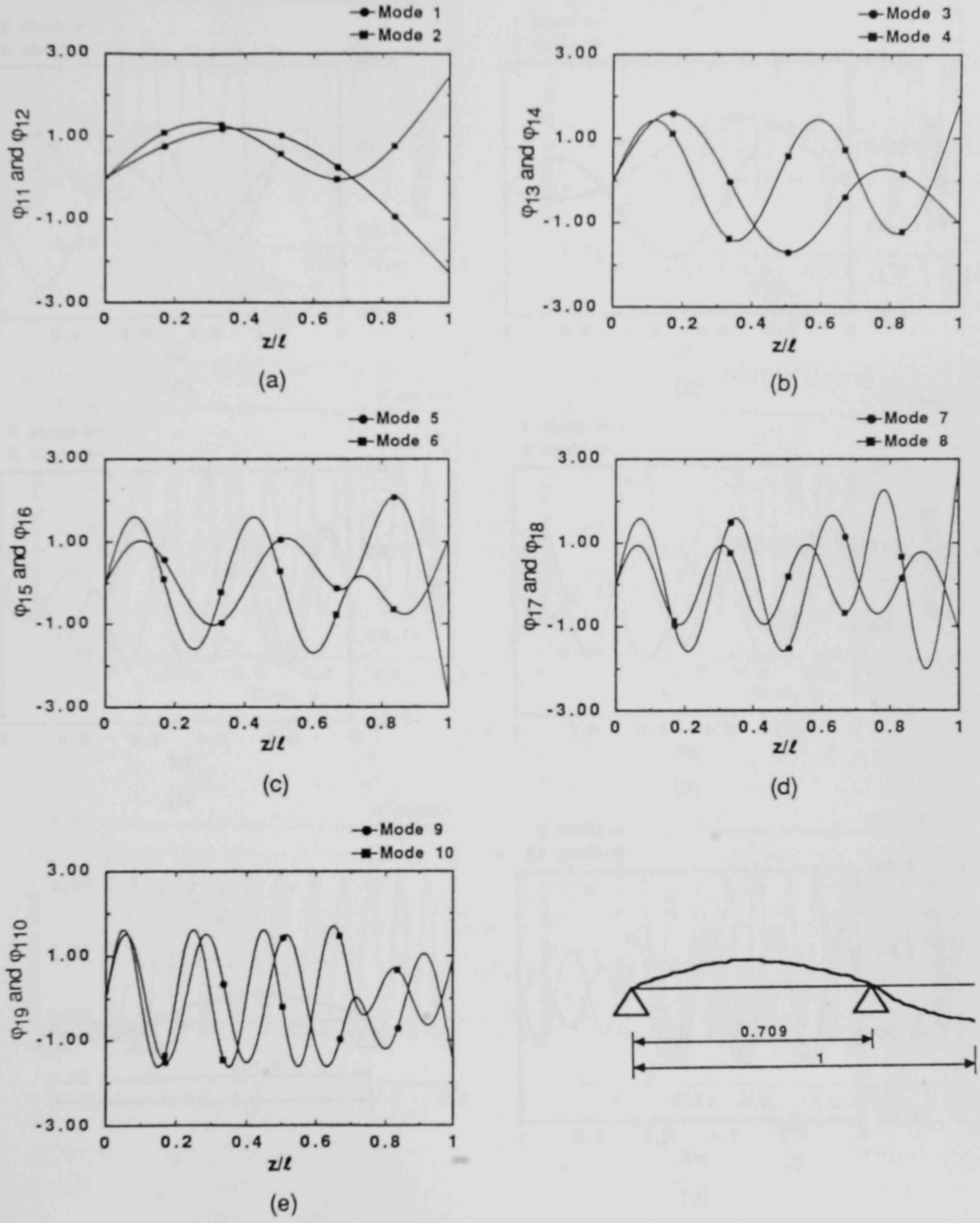

Fig. 7. Mode shapes for Model 1

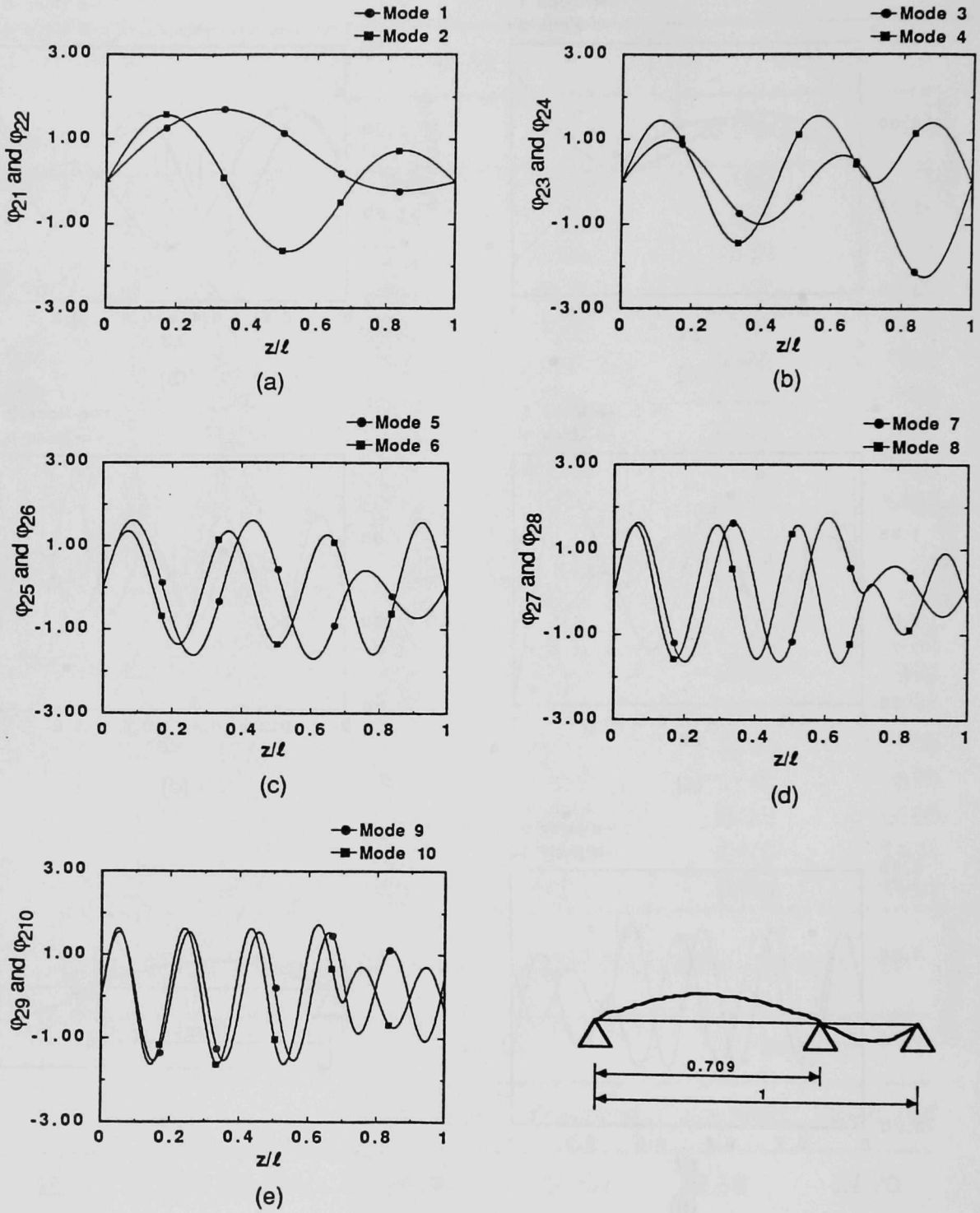

Fig. 8. Mode shapes for Model 2

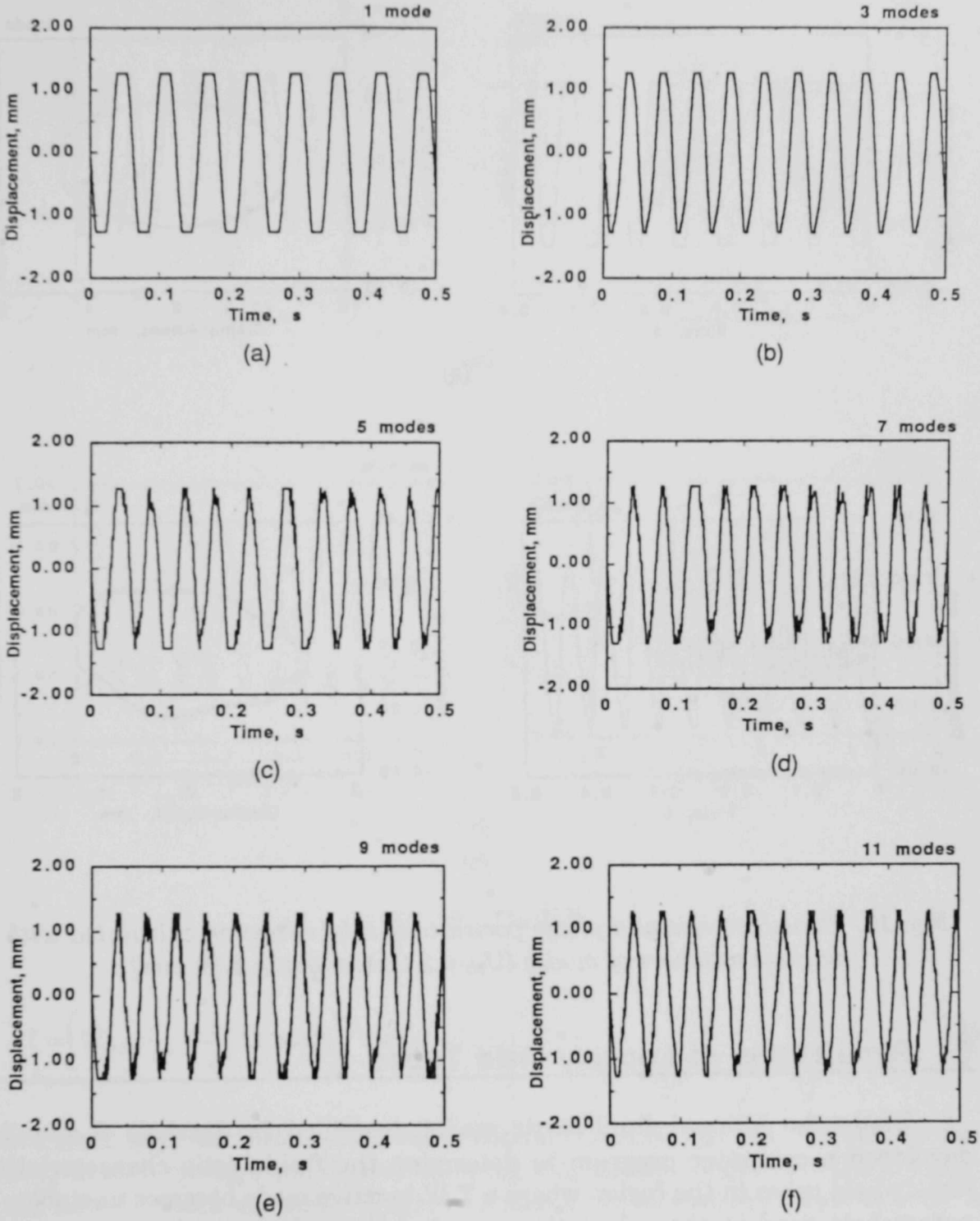

Fig. 9. Time histories of tube displacement calculated with various numbers of modes (U_m = 2.0 m/s, gap = 2.54 mm)

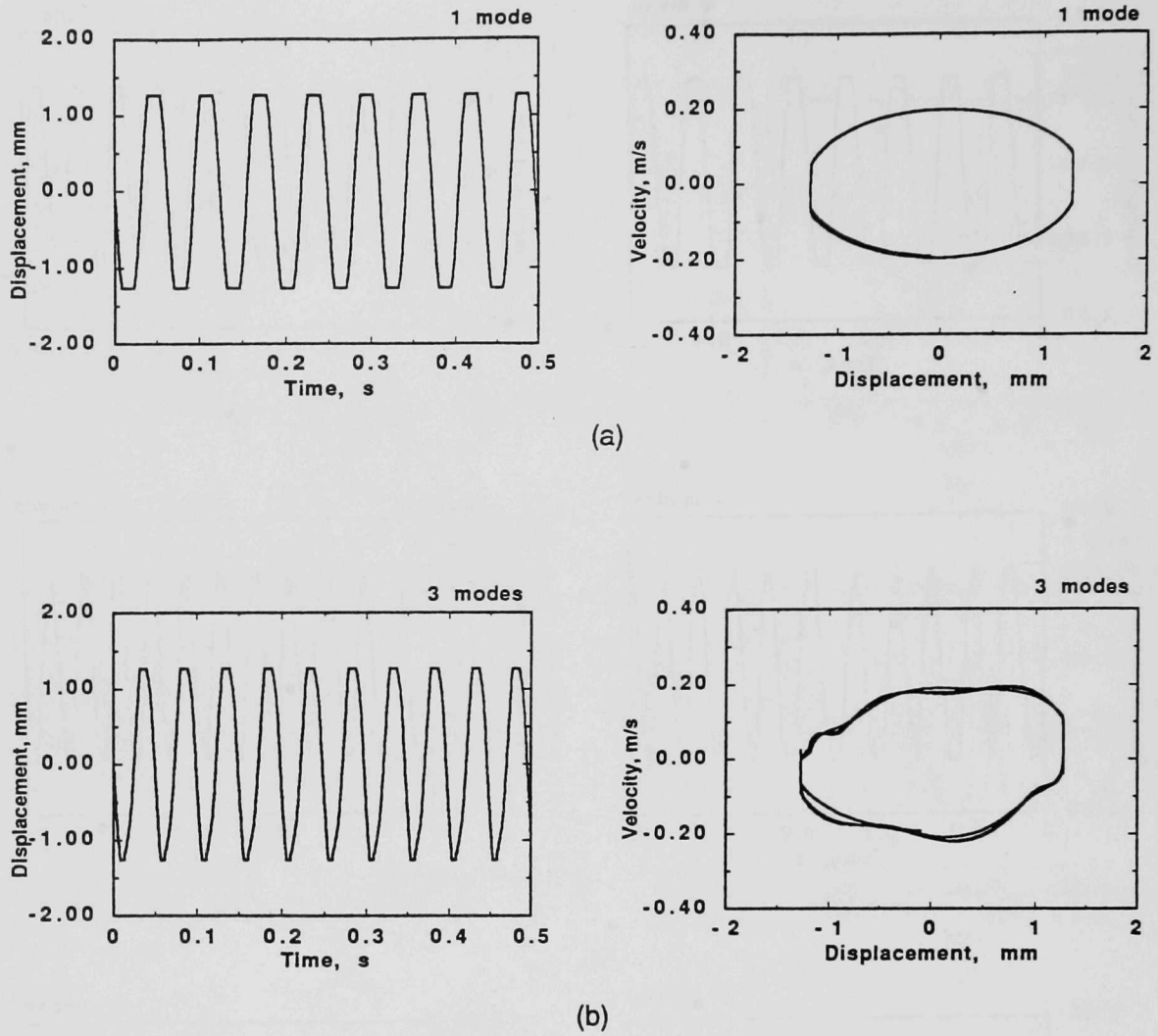

Fig. 10. Time histories and phase portraits of tube vibration calculated with various numbers of modes (U_m = 2.0 m/s, gap = 2.54 mm)

5 Simulations of Loosely Held Tubes

Using the bilinear fluidelastic model described in Sections 2 and 3, we developed a computer program to determine the fluidelastic characteristics of loosely held tubes in the region where a TSP-inactive mode becomes unstable. The parameters used in the calculations are based on those in the experiments of Chen et al.[1] (Fig. 2).

It is obvious that flow velocity plays an important role in fluidelastic instability. According to Eqs. 6, the system damping depends on flow velocity and fluid force coefficients, namely

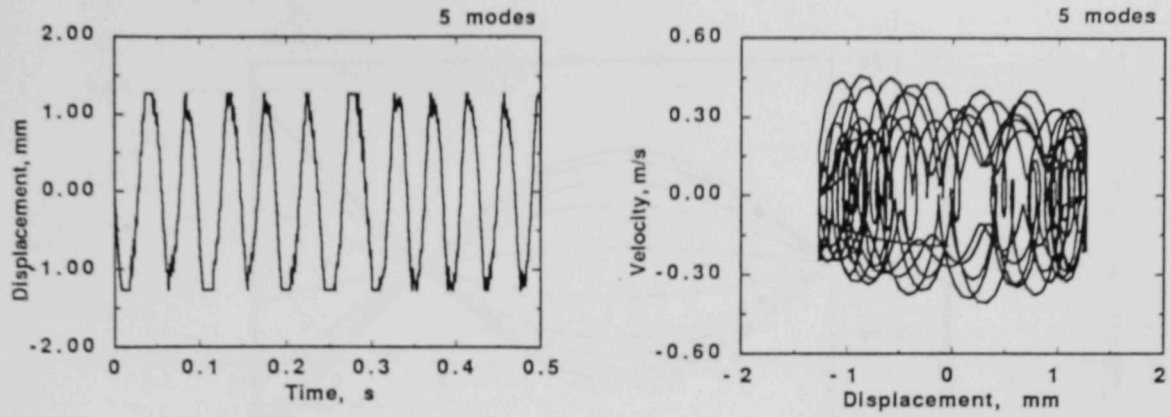

(c)

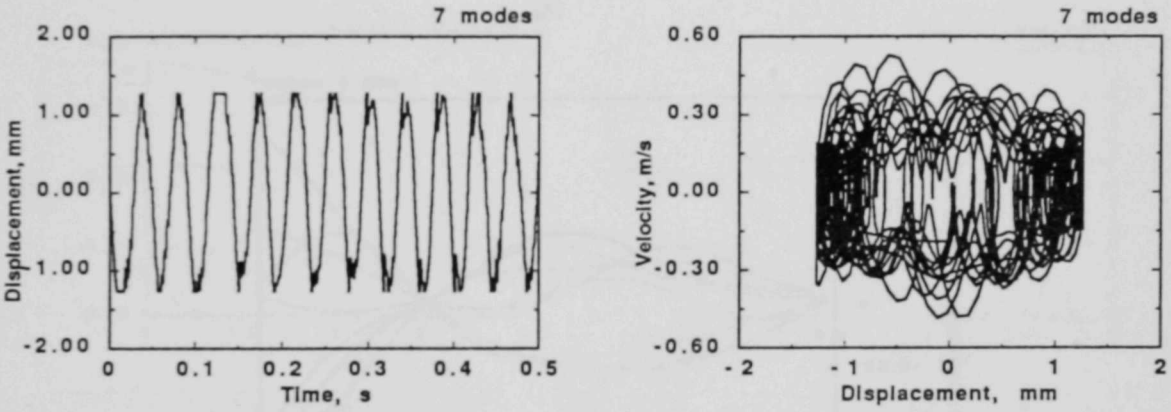

(d)

Fig. 10. (Cont'd)

$$\zeta = \left(2\zeta_{jn}\omega_{jn} - \frac{\gamma_j}{\pi^3} U_r^2 \omega \alpha_{jj}^d \right) / (2\omega), \tag{47}$$

where fluid force coefficients are also functions of flow velocity. When the flow velocity is high enough, the system damping may become negative and the motion of the tube becomes unstable. Figure 12 shows the influence of flow velocity on system damping for the first two modes of both Models 1 and 2. (Calculations indicated that the flow velocity, which ranges from 1-150 m/s, will not have much effect on the higher modes.) In Fig. 12, the damping varies largely with flow velocity only at the first two modes of Model 1 and at the first mode of Model 2.

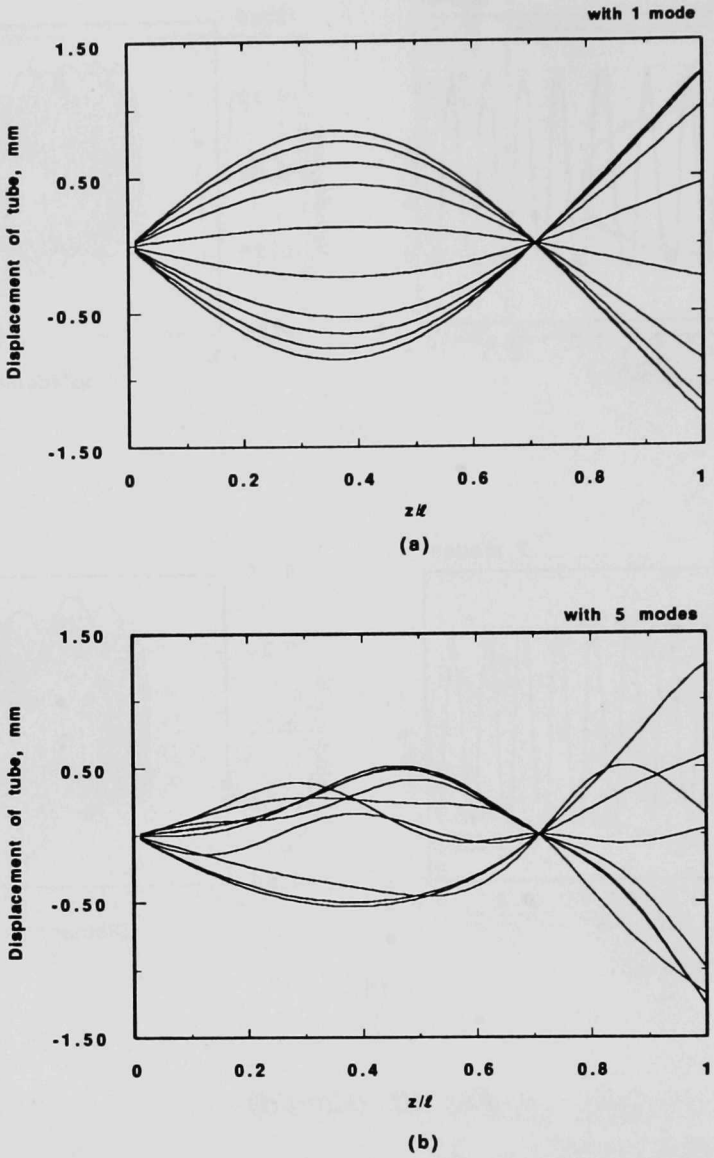

Fig. 11. Mode shapes of tube motion in one cycle (U_m = 2.0 m/s, gap = 2.54 mm)

This indicates that fluidelastic instability occurs at the lower modes. In our case, the motion of the tube becomes unstable when the flow velocity is over 1.5 m/s. This velocity is the critical flow velocity at which the damping is equal to zero (see Fig. 12).

The oscillating frequency in Eq. 11 is calculated for different flow velocities with the iterative method. The results are shown in Fig. 13, which shows that, when a TSP-inactive mode becomes unstable (flow velocity greater than 1.5 m/s),

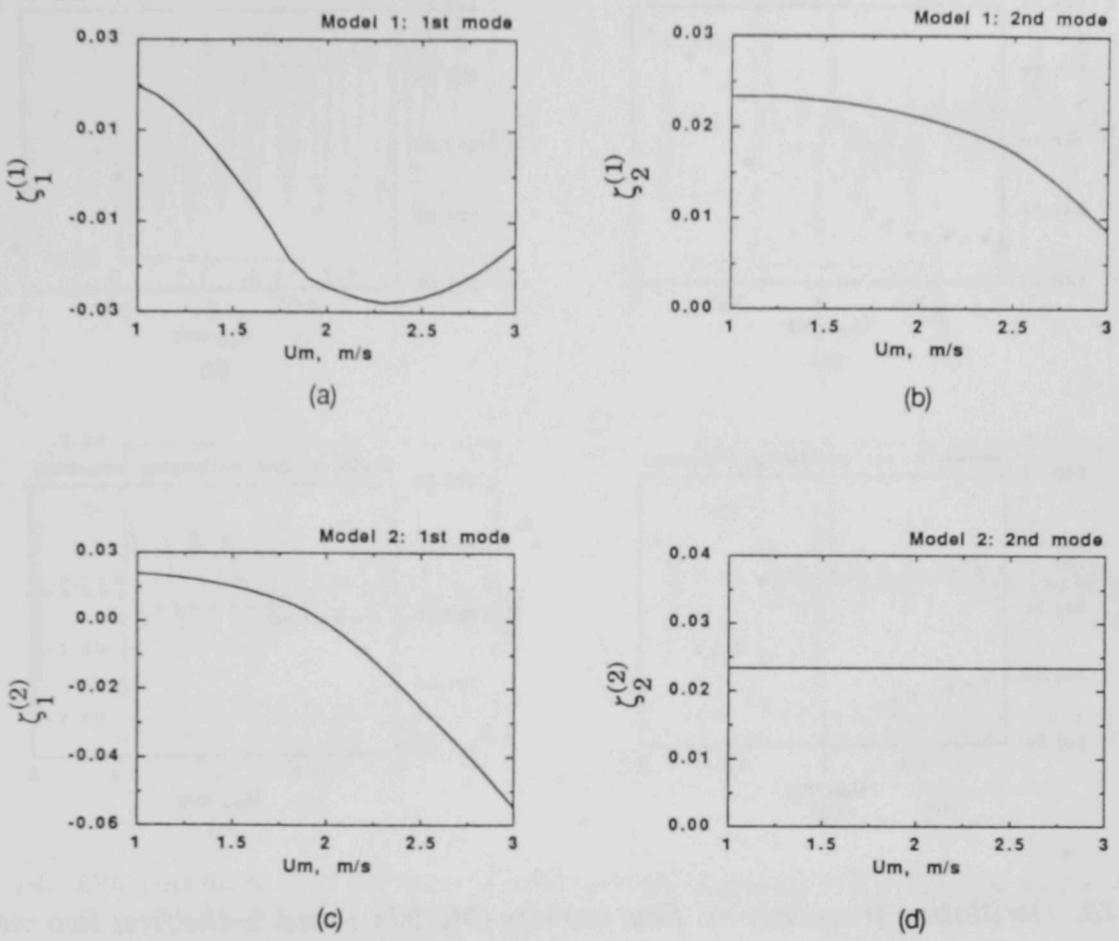

Fig. 12. Modal damping vs. flow velocity (Models 1 and 2, at the first two modes)

the fundamental oscillating frequency increases with increasing flow velocity (Fig. 13a).

Figure 14 shows the time histories of tube oscillations (displacement and velocity of a tube) at point C3 (Figs. 2-4) (z/ℓ = 1.0) and point (z/ℓ = 0.35), the midspan between C1 and C2 (Figs. 2-4) for U_m = 2.0 m/s and $e_1 = e_2$ = 2.54 mm. At this flow velocity, the modal damping of the TSP-inactive mode is negative and the tube is unstable. Tube oscillation amplitudes increase until the tube strikes the TSP at the right end, C3. Once this occurs, tube boundary conditions are changed, and the tube frequencies, modal damping, and stiffness increase. The tube is stabilized, oscillation amplitudes are reduced, and the tube loses contact with the stop at C3. Therefore, the tube goes back to the original state associated with the instability of the first TSP-inactive mode. The tube oscillations will go through the same cycles again. When the tube motion changes between Models 1 and 2, large changes occur in the velocity.

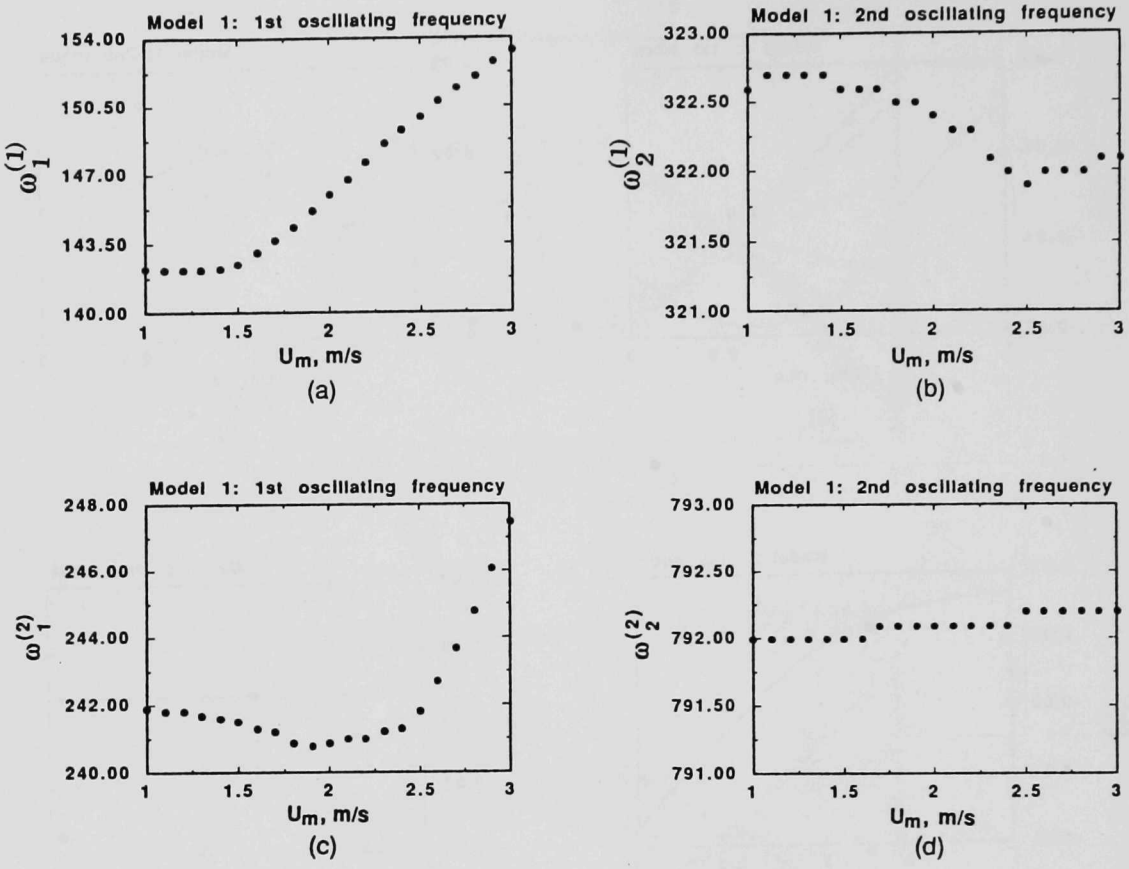

Fig. 13. Oscillation frequency vs. flow velocity (Models 1 and 2, the first two modes)

Figure 15 shows time histories of tube displacement at different flow velocities and phase portraits of tube motion when the initial conditions are the same. When flow velocity is lower than critical flow velocity, damping of the system is positive, motion is stable, and oscillation amplitudes decrease with time (Fig. 15a, U_m = 1.0 m/s). When flow velocity is equal to critical flow velocity, U_m = 1.5 m/s, oscillation amplitudes remain the same, and the phase portrait is an ellipse (Fig. 15b). When flow velocity is larger than critical flow velocity (Fig. 15c, U_m = 1.8 m/s), damping becomes negative, and the tube becomes unstable. Its amplitudes increase until the right end reaches the TSP. Its phase portrait is very complicated.

Figure 16 shows a plot of the ratio of RMS tube displacement to tube diameter vs. flow velocity for different stop clearances. Tube response characteristics here include two regions: low-amplitude oscillation and instability of the TSP-inactive mode.

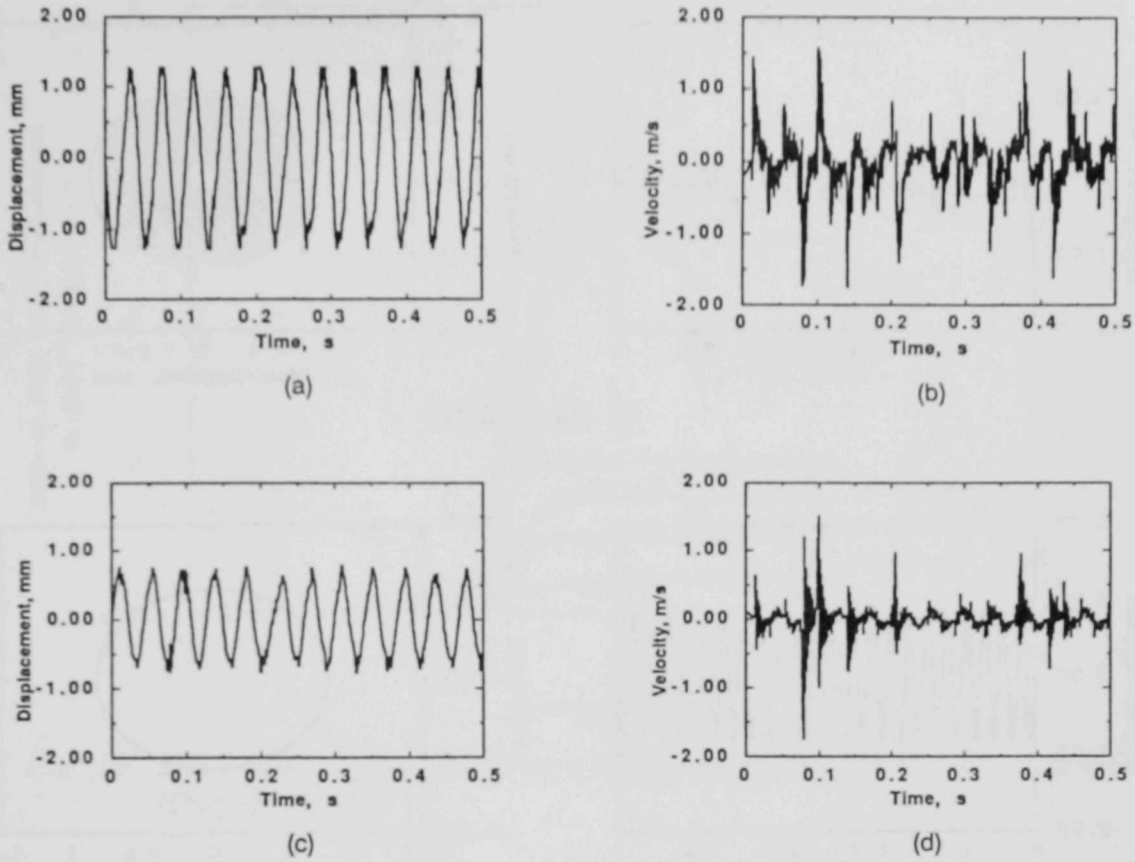

Fig. 14. Displacement and velocity of tube motion at points $z/\ell = 1.0$ and $z/\ell = 0.35$ ($U_m = 2.0$ m/s, gap = 2.54 mm))

In the low-amplitude-oscillation region (for flow velocity lower than 1.5 m/s), the tube motion is small and the tube responds in the TSP-inactive mode.

In the instability region of the TSP-inactive mode, as the flow velocity increases to the critical flow velocity, the TSP-inactive mode becomes unstable. Once the tube loses its stability, large amplitude oscillations occur and the tube impacts the TSP. Therefore, the maximum peak-to-peak displacement at the TSP is that of the diametral clearance. In this range of flow velocity, tube displacement is almost independent of flow velocity because the motion shifts into a stable TSP-inactive mode when a tube impacts the TSP. From Fig. 16, we see that the results from the simulation by the bilinear fluidelastic model agree reasonably well with the experimental data of Chen et al.[1] Figure 17 shows a plot of the ratio of RMS tube displacement to tube diameter vs. flow velocity at transducer points A and B (Fig. 2) when the diametral clearance is 1.02 mm. Because the TSP-inactive model is dominant, the RMS displacement value at point A is always larger than that at point B. (If the TSP-active model is

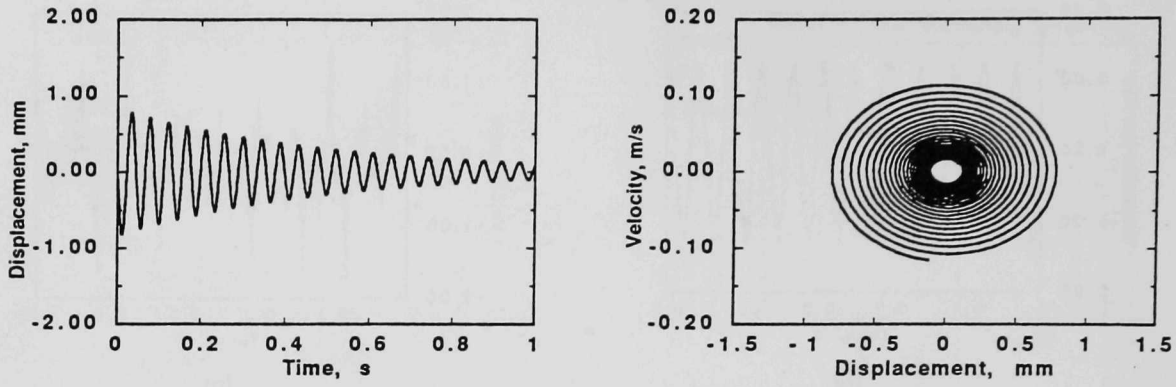

(a) U_m = 1.0 m/s

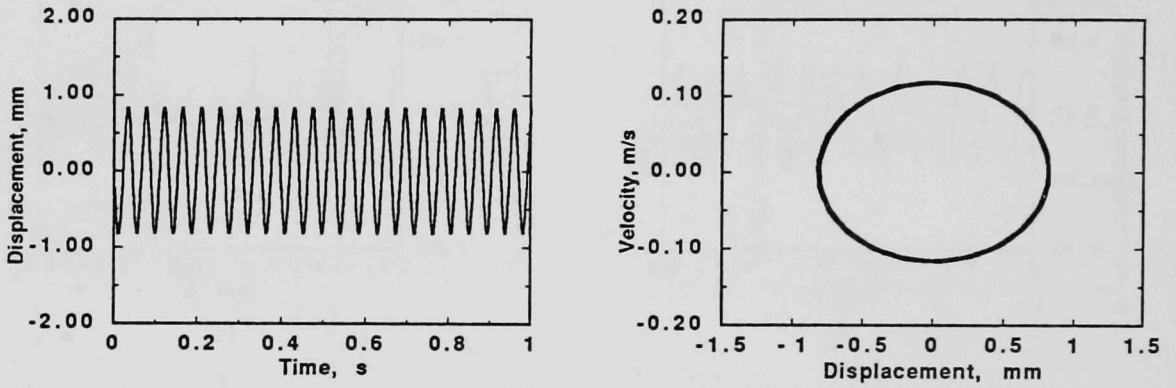

(b) U_m = 1.5 m/s

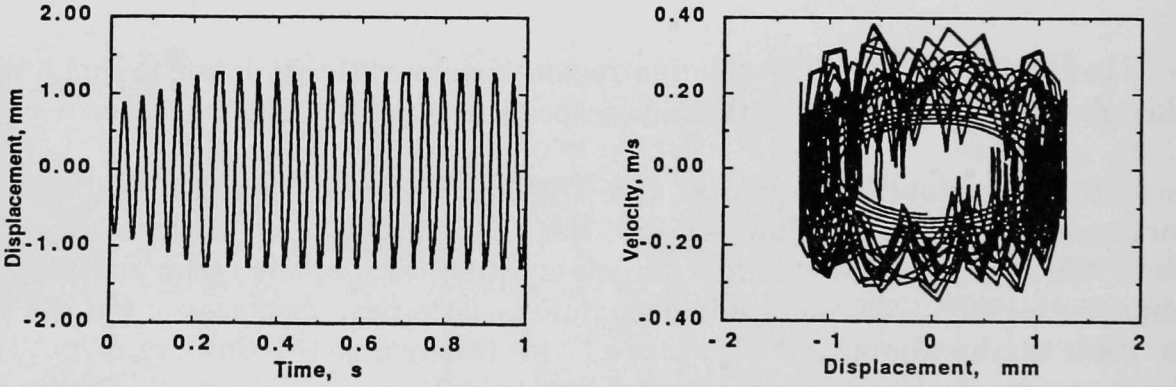

(c) U_m = 1.8 m/s

Fig. 15. Time histories of displacement and portraits of tube motion at various flow velocities (gap = 2.54 mm)

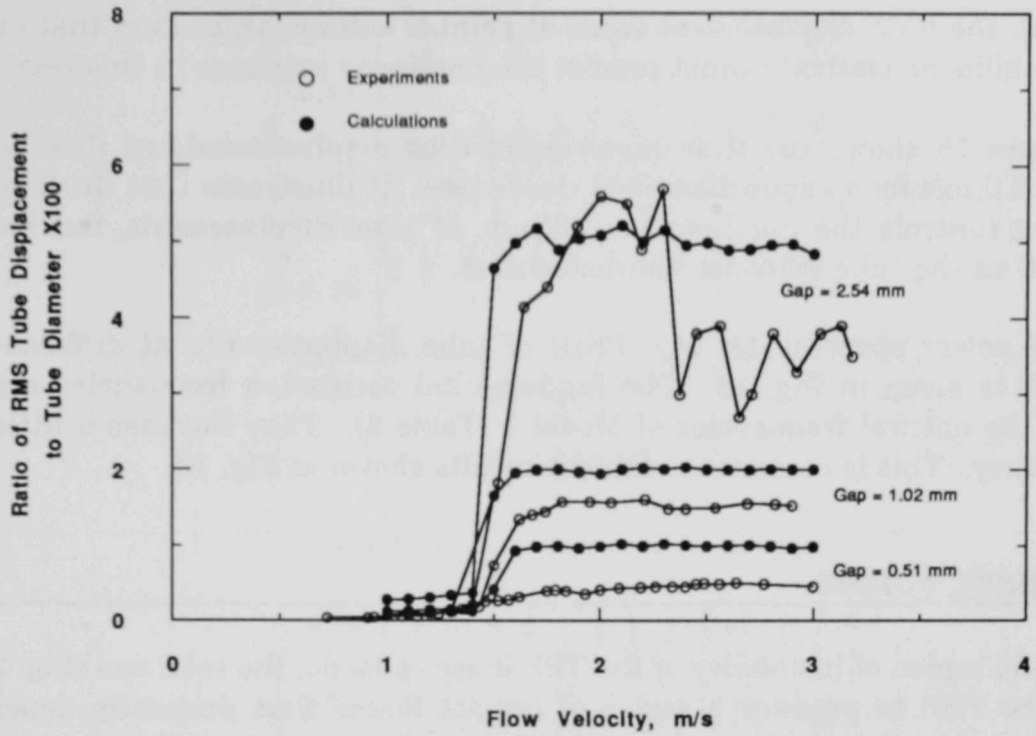

Fig. 16. RMS tube displacement as a function of flow velocity for various diametral gaps

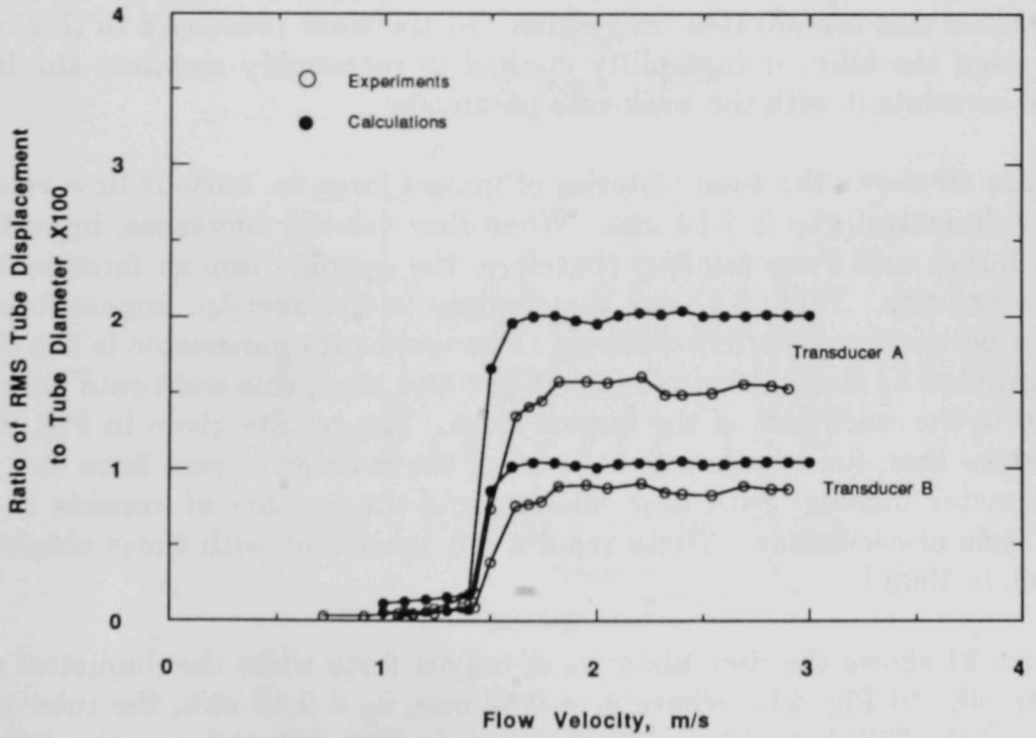

Fig. 17. RMS tube displacement as a function of flow velocity with a diametral gap of 1.02 mm

dominant, the RMS displacement value at point B will be larger than that at point A.[1] The bilinear method cannot predict the nonlinear response in this region.)

Figure 18 shows the time histories of tube displacements at flow velocity equal to 2.0 m/s for various diametral clearances. It illustrates that the diametral clearance controls the maximum amplitude of tube displacement, but has less influence on the tube response characteristics.

The power spectral density (PSD) of tube displacements at different flow velocities is given in Fig. 19. The fundamental oscillation frequencies are very close to the natural frequencies of Model 1 (Table 2). They increase a little with flow velocity. This is consistent with the results shown in Fig. 13.

6 Impact Forces

In the region of instability of the TSP-inactive mode, the tube end (Fig. 2) will strike the TSP to produce a series of impact forces that primarily depend on tube/support parameters, such as contact time, contact stiffness, and fluid squeeze film. The process of a tube striking a TSP affects tube wear. We know that the detailed dynamics of tube/support interaction are extremely complicated. In future work, we will consider additional theoretical and experimental studies to understand this complicated interaction. In the work presented in this report, we only used the bilinear instability method to reasonably simulate the impact force and correlate it with the work-rate parameter.

Figure 20 shows the time histories of impact force vs. various flow velocities when the diametral gap is 2.54 mm. When flow velocity increases, impact force becomes larger and more regular; therefore, the average impact force increases with flow velocity. Table 3 shows the changes in the average impact force and work-rate parameter with flow velocity. The work-rate parameter is the impact force multiplied by the number of impacts per unit time; this work-rate parameter is related to the work rate of the impact force. The results given in Fig. 20 and Table 3 show that, for a large gap (2.54 mm), the average impact force and work-rate parameter increase with flow velocity, and the number of impacts is about two per cycle of oscillation. These results are consistent with those obtained by Chen et al. in 1983.[1]

Figure 21 shows the time histories of impact force when the diametral gap is asymmetrical. In Fig. 21a, where e_1 = 0.50 mm, e_2 = 0.45 mm, the tube strikes both sides of the TSP but with a different force; in Figs. 21b and c, as the difference of gap on the two sides is increased, the tube strikes only the side of the TSP where the gap is smaller.

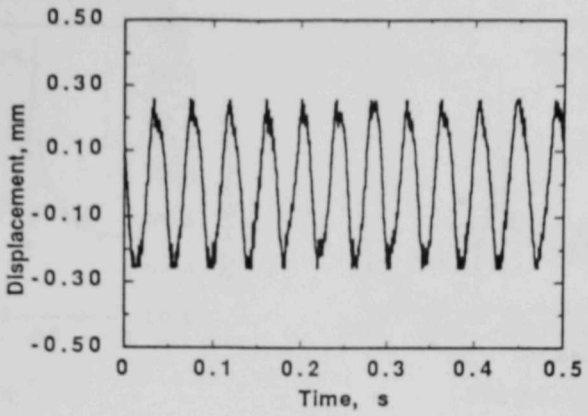

(a) Gap = 0.51 mm

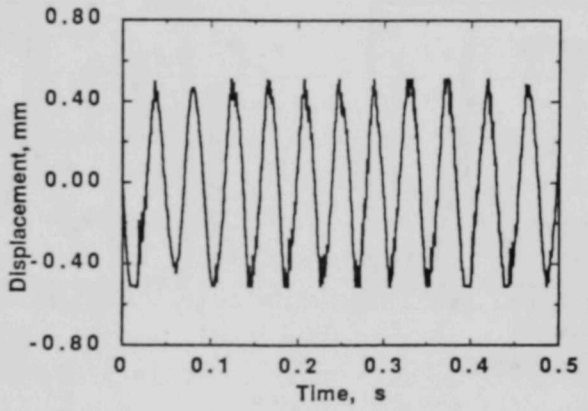

(b) Gap = 1.02 mm

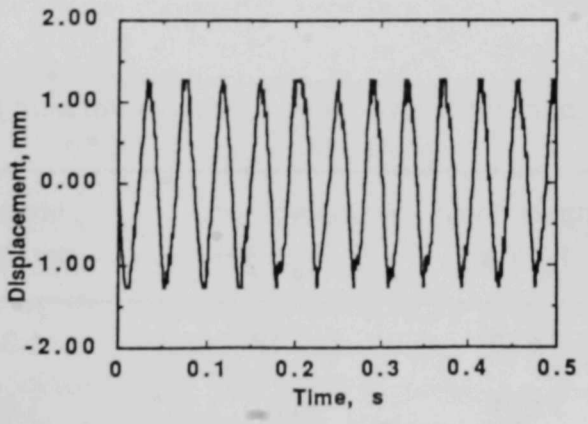

(c) Gap = 2.54 mm

Fig. 18. Time histories of tube displacements for various gaps (U_m = 2.0 m/s)

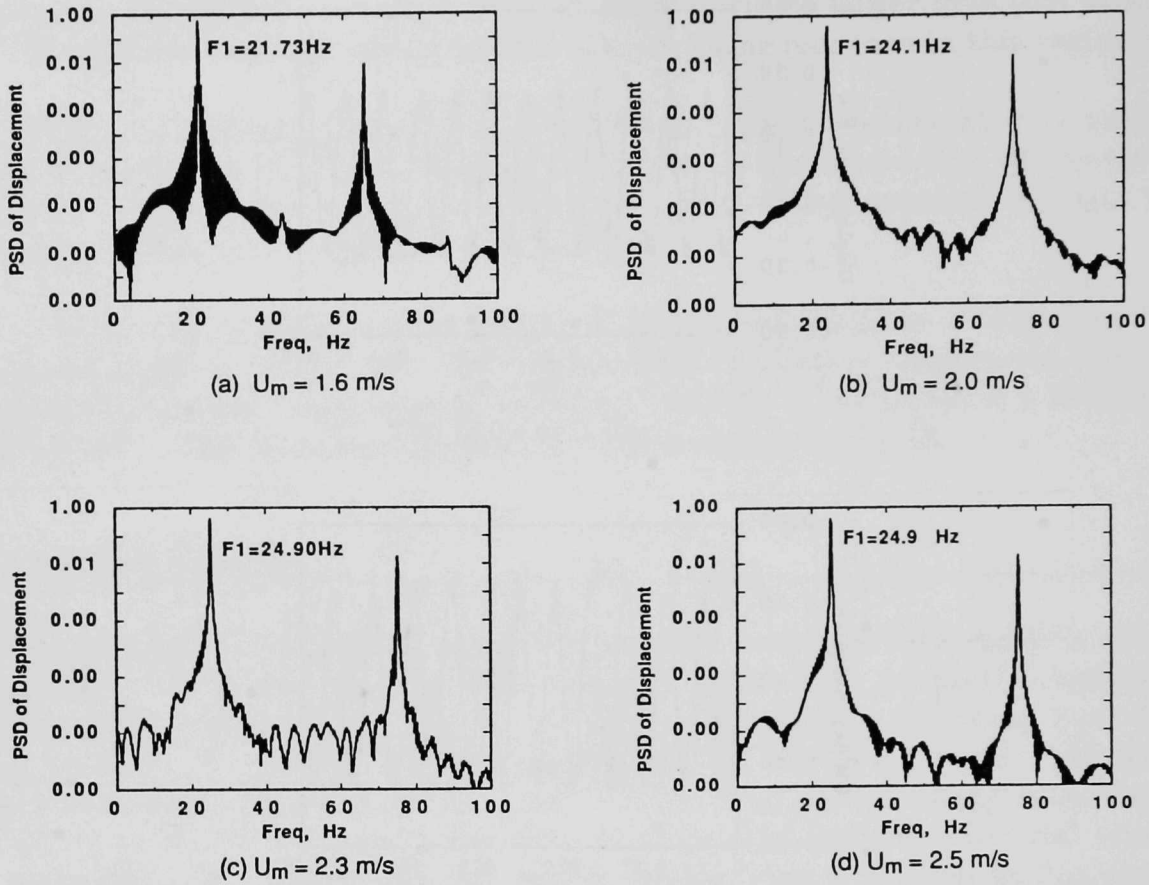

Fig. 19. PSD of tube displacement for various flow velocities when the diametral gap is 2.54 mm

Table 3. Impact force and work rate with various flow velocities

Flow Velocity U_m (m/s)	Impact Force F_i (N)	Contact Time T_c (%)	Impacts per Cycle	Work-rate Parameter W_r
1.8	6.626	11.18	1.88	12.46
2.0	7.281	10.67	1.88	13.69
2.2	7.484	10.68	1.88	14.09
2.5	7.683	11.19	1.97	15.15

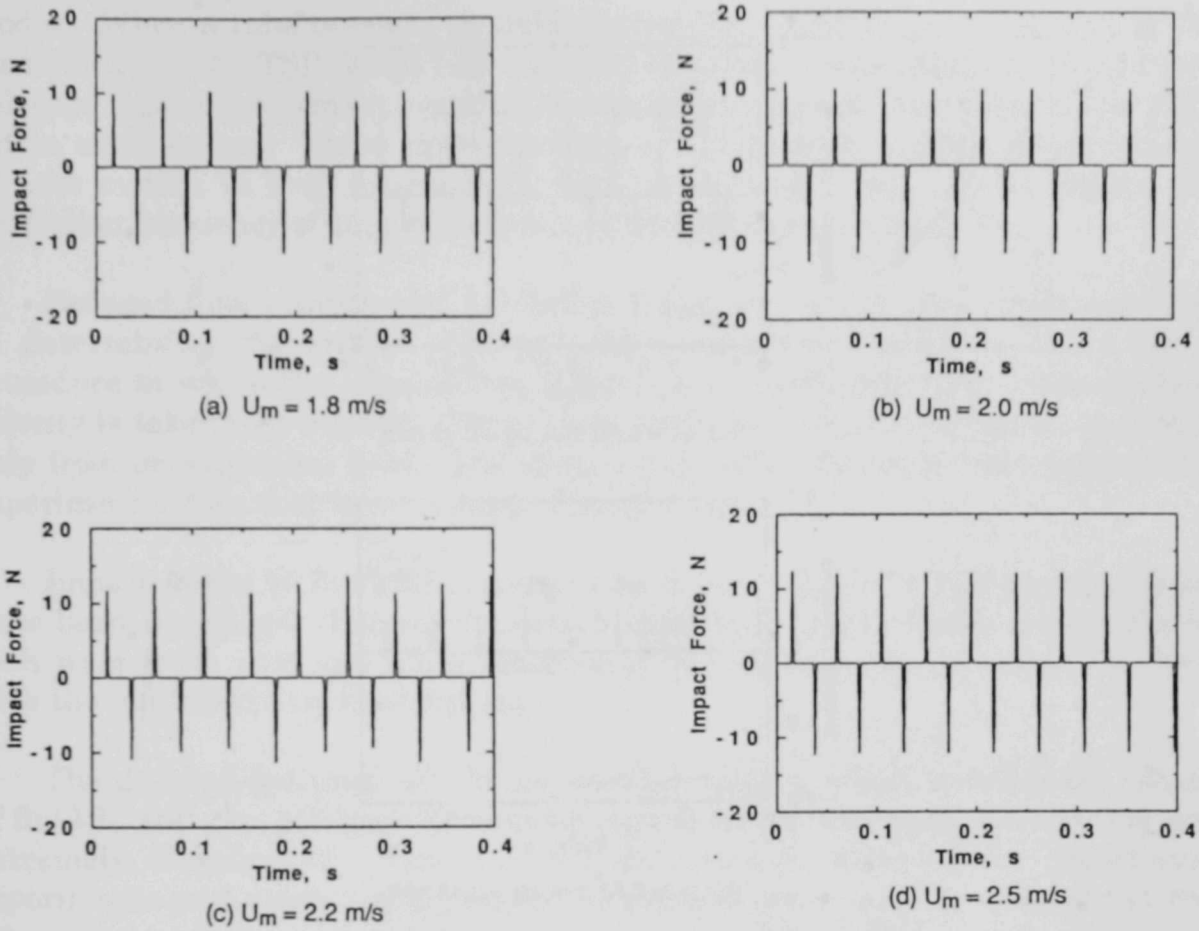

Fig. 20. Time histories of impact force with various flow velocities (gap = 2.54 mm)

7 Conclusions

In this report, a mathematical methodology based on the unsteady flow theory and linear modal analysis technique is presented for fluidelastic instability of loosely supported tubes subjected to nonuniform crossflow. The simulation, when compared with prior experimental data, shows that this methodology is applicable for predicting the fluidelastic instability response of a tube when the TSP-inactive mode becomes unstable. However, it is not applicable for the instability region associated with TSP-active modes because, once a TSP-active mode becomes unstable, other nonlinear effects become important and those effects are not included in this model. Those nonlinear effects will be incorporated in the model in future studies.

Tube response characteristics associated with instability of the TSP-inactive mode are different from other types of excitation and those of the TSP-active

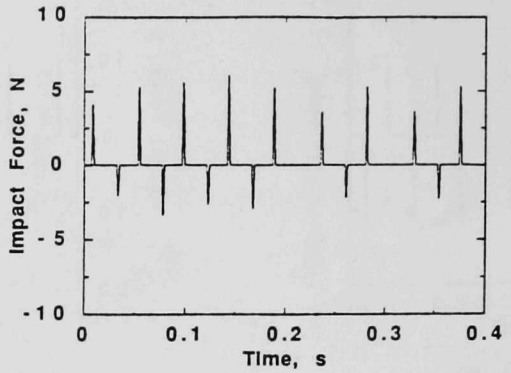

(a) e_1 = 0.50 mm, e_2 = 0.45 mm

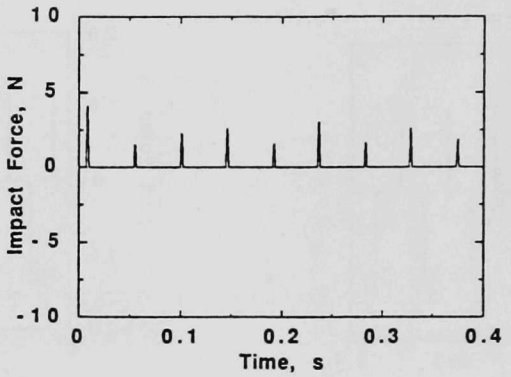

(b) e_1 = 0.55 mm, e_2 = 0.45 mm

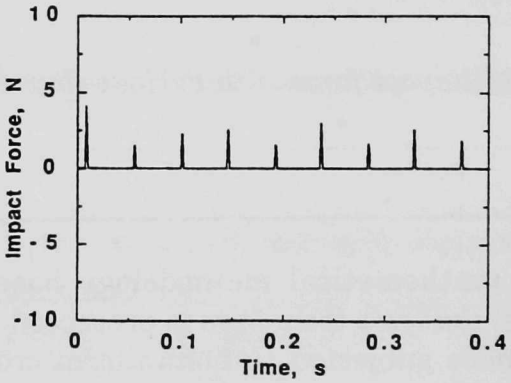

(c) e_1 = 0.60 mm, e_2 = 0.45 mm

Fig. 21. Time histories of impact force with various asymmetrical gaps at flow velocity U_m = 2.0 m/s

modes. When a tube becomes unstable in the TSP-inactive mode, because of the constraints at the TSP, large tube oscillations do not occur. With increased flow velocity, tube displacement remains almost constant until instability of the TSP-active mode occurs. These characteristics are illustrated in RMS displacements of tube motion in both experiments and simulations. But, in this region, the oscillation frequency of tube motion increases with flow velocity.

Reduced flow velocity and oscillation frequency, which play important roles in determining the critical flow velocity, can be estimated by an iterative procedure in which the relationship of fluid-force coefficients to the reduced flow velocity is taken into account. These force coefficients at present can be evaluated only from experimental data. The work presented in this report is based on the experimental data that is available in the literature.

Impact forces at the TSP associated with instability of a TSP-inactive mode have been simulated. The results, which show that impact forces are correlated with wear work rate and are a function of flow velocity, agree reasonably well with the published experimental data.

The detailed dynamics of tube/support interaction, which includes the effects of fluid in the gap, stiffness of support, impact forces, and wear mechanism, are extremely complicated. They are not discussed in this report. Additional experiments and analytical/numerical procedures are needed to understand the interaction process and its effects on tube wear and life prediction in the future.

Acknowledgments

This work was cosponsored by the Northeast Utilities Service Company and the U.S. Department of Energy, Office of Conservation and Renewable Energy, Advanced Industrial Concepts Division, under Contract W-31-109-Eng-38. The work also represents a U.S. contribution to the International Energy Agency (IEA) Program of Research and Development on Energy Conservation in Heat Transfer and Heat Exchangers.

References

1. Chen, S. S., Jendrzejczyk, J. A., and Wambsganss, M. W., *Dynamics of Tubes in Fluid with Tube-Baffle Interaction,* ASME Symp. on Flow-Induced Vibration, New Orleans, Vol. 2, pp. 285-304 (1984).

2. Haslinger, K. H., Martin, M. L., and Steininger, D. A., *Pressurized Water Reactor Steam Generator Tube Wear Prediction Utilizing Experimental Techniques,* International Conf. on Flow Induced Vibration, Bowness-on-Windermere, England, Paper K2, pp. 437-448 (1987).

3. Antunes, J., Axisa, F., Beaufils, B., and Guilbaud, D., *Coulomb Friction Modelling in Numerical Simulations of Vibration and Wear Work Rate of Multispan Tube Bundles,* International Symp. on Flow Induced Vibration and Noise, Chicago, Vol. 5, pp. 157-176 (1988).

4. Godon, J. L., and Lebret, J., *Influence of the Tube-Support Plate Clearance on Flow-Induced Vibration in Large Condensers,* International Symp. on Flow Induced Vibration and Noise, Chicago, Vol. 5, pp. 177-186 (1988).

5. Yeh, Y. S., and Chen, S. S., *Flow-Induced Vibration of Component Cooling Water Heat Exchangers,* ASME Pressure Vessels and Piping Conf., Nashville, TN, PVP Vol. 189, pp. 153-163 (1990).

6. Yu, X., *An Analysis of Tube Failure in a U-shape Tube Bundle,* ASME Pressure Vessels and Piping Conf., Chicago, PVP Vol. 104, pp. 187-192 (1986).

7. Fisher, N. J., and Ingham, B., *Measurement of Tube-to-Support Dynamic Force in Fretting-Wear Rigs,* International Symp. on Flow Induced Vibration and Noise, Chicago, Vol. 5, pp. 137-156 (1988).

8. Haslinger, K. H., Martin, M. L., and Steininger, D. A., *Experimental Characterization of Fluid and Squeeze Film Effects in Heat Exchanger Tube Supports,* Flow-Induced Vibration – 1989, ASME Pressure Vessels and Piping Conf., PVP-Vol. 154, pp. 31-41 (1989).

9. Ko, P. L., and Magel, E., *Impact and Sliding Wear in Steam Generators and Heat Exchangers: New Experimental Test Rig and Wear Model,* Flow-Induced Vibration – 1989, ASME Pressure Vessels and Piping Conf., PVP-Vol. 154, pp. 63-69 (1989).

10. Nakamura, T., and Fujita, K., *A Study on Impact Vibration of Loosely Held Tube by Cross Flow,* International Conf. on Flow Induced Vibration, Bowness-on-Windermere, England, Paper K1, pp. 427-436 (1987).

11. Antunes, J., Axisa, F., and Vento, M. A., *Experiments on Vibro-Impact Dynamics Under Fluidelastic Instability,* ASME Pressure Vessels and Piping Conf., Nashville, TN, PVP-Vol. 189, pp. 127-138 (1990).

12. Rao, M. S. M., et al., *Computer Modelling of Vibration and Wear of Multispan Tubes with Clearances at Tube Supports,* International Conf. on Flow Induced Vibration, Bowness-on-Windermere, England, Paper K3, pp. 449-466 (1987).

13. Fisher, N. J., Olesen, M. J., Rogers, R. J., and Ko, P. L., *Simulation of Tube-to-Support Dynamic Interaction in Heat Exchange Equipment,* International Symp. on Flow Induced Vibration and Noise, Chicago, Vol. 5, pp. 121-136 (1988).

14. Fricker, A. J., *Numerical Analysis of the Fluidelastic Vibration of a Steam Generator Tube with Loose Supports,* International Symp. on Flow Induced Vibration and Noise, Chicago, Vol. 5, pp. 105-120 (1988).

15. Rao, M. S. M., Steininger, D. A., and Eisinger, F. L., *Numerical Simulation of Fluidelastic Vibration and Wear of Multispan Tubes with Clearances at Supports,* International Symp. on Flow Induced Vibration and Noise, Chicago, Vol. 5, pp. 235-250 (1988).

16. Goyder, N. G. D., and Teh, C. E., *A Study of the Impact Dynamics of Loosely Supported Heat Exchanger Tubes,* International Symp. on Flow Induced Vibration and Noise, Chicago, Vol. 5, pp. 87-104 (1988).

17. Eisinger, F. L., Rao, M. S. M., and Steininger, D. A., *Numerical Simulation of Fluid Instability of Multispan Tubes Partially Exposed to Crossflow,* Trans. 10th SMiRT, Vol. T, pp. 45-56 (1989).

18. Andjelic, M., Austermann, R., and Popp, K., *Multiple Stability Boundaries of Tubes in a Normal Triangular Cylinder Array,* ASME Pressure Vessels and Piping Conf., Nashville, TN, PVP-Vol. 189, pp. 87-98 (1990).

19. Chen, S. S., and Jendrzejczyk, J. A., *Characteristics of Fluidelastic Instability of Tube Row In Crossflow,* International Conf. on Flow Induced Vibration, Bowness-on-Windermere, England, Paper B3, pp. 77-84 (1987).

20. Axisa, F., Antunes, J., and Villard, B., *Overview of Numerical Methods for Predicting Flow-Induced Vibration,* Trans. ASME Pressure Vessels and Piping, Vol. 110, pp. 6-14 (1988).

21. Andjelic, M., and Popp, K., *Stability Effects in a Normal Triangular Cylinder Array,* J. Fluid Structure, Vol. 3, pp. 165-185 (1989).

22. Chen, S. S., *Some Issues Concerning Fluidelastic Instability of a Group of Circular Cylinders in Cross-Flow,* Trans. ASME, J. Press. Vessel Technol., Vol. 111, pp. 507-518 (1989).

23. Chen, S. S., and Chandra, S., *Fluidelastic Instabilities in Tube Bundles Exposed to Nonuniform Crossflow,* ASME Pressure Vessels and Piping Conf., Nashville, TN, PVP-Vol. 189, pp. 65-77 (1990).

24. Tanaka, M., *Study on Fluidelastic Vibrations of Tube Bundle,* Jpn. Soc. Mech. Eng., Trans., Section B, Vol. 46(408), pp. 1398-1407 (1980).

25. Chen, S. S., and Jendrzejczyk, J. A., *Stability of Tube Arrays in Crossflow,* Nucl. Eng. Des., Vol. 75(3), pp. 351-374 (1983).

Distribution for ANL–90/38

Internal

K. J. Bell
Y. Cai (5)
S. S. Chen (5)
H. Drucker
J. A. Jendrzejczyk
C. A. Malefyt
T. M. Mulcahy
C. B. Panchal
T. J. Rabas
W. W. Schertz
Y. W. Shin
A. Thomas
R. A. Valentin
M. W. Wambsganss (3)
R. W. Weeks
ANL Patent Dept.
ANL Contract File
TIS Files (3)

External

DOE–OSTI for distribution per UC–310 (119)
ANL–TIS Libraries
Manager, Chicago Operations Office, DOE
Director, Technology Management Div., DOE–CH
D. L. Bray, DOE–CH
A. L. Taboas, DOE–CH
Materials and Components Technology Division Review Committee:
- H. Berger, Industrial Quality, Inc., Gaithersburg, MD
- M. S. Dresselhaus, Massachusetts Institute of Technology, Cambridge, MA
- S. J. Green, Electric Power Research Institute, Palo Alto, CA
- R. A. Greenkorn, Purdue University, West Lafayette, IN
- C.–Y. Li, Cornell University, Ithaca, NY
- P. G. Shewmon, Ohio State University, Columbus
- R. E. Smith, Electric Power Research Institute, NDE Ctr., Charlotte, NC

M. E. Gunn, DOE, Washington, DC (2)
S. Chandra, Northeast Utilities Service Co. (5)
M. Pitek, Northeast Utilities Service Co. (5)